Article

Cell Reports

The SNARE VAMP7 Regulates Exocytic Trafficking of Interleukin-12 in Dendritic Cells

Graphical Abstract

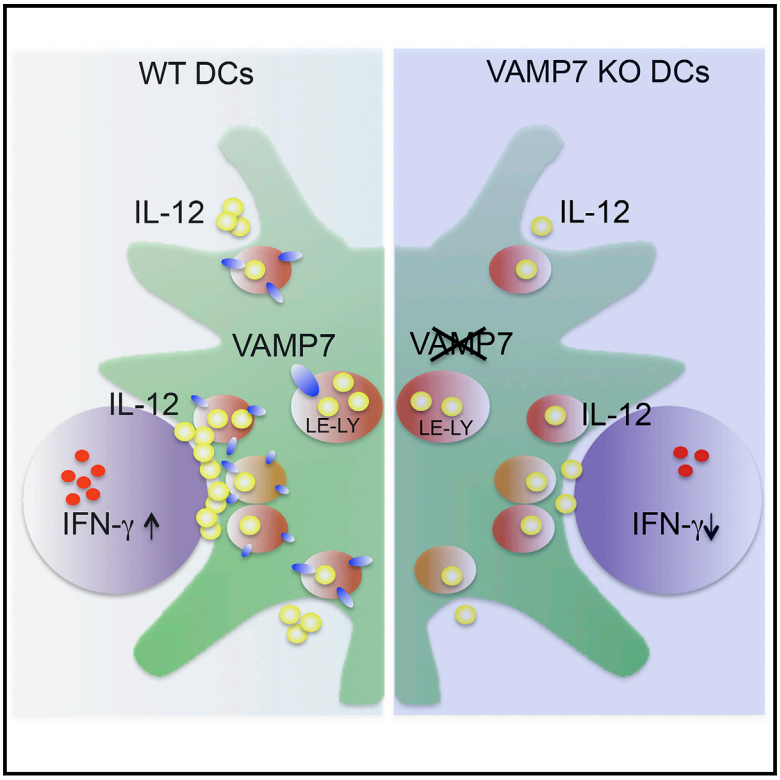

Authors

Giulia Chiaruttini, Giulia M. Piperno, Mabel Jouve, ..., Salvatore Valitutti, Thierry Galli, Federica Benvenuti

Correspondence

benvenuti@icgeb.org

In Brief

Efficient priming of T cells requires antigenic and soluble cytokine signals. Chiaruttini et al. analyze the intracellular trafficking pathway of IL-12 in dendritic cells and identify the SNARE VAMP7 as a key regulator of cytokine release and T cell activation.

Highlights

- Intracellular trafficking of IL-12 in dendritic cells is mediated by the SNARE VAMP7
- VAMP7 is required for optimal secretion of IL-12 in the extracellular space
- IL-12/VAMP7^{+} vesicles gather at the immune synapse
- VAMP7 controls synaptic release of IL-12 and IFN-γ production in T cells

Chiaruttini et al., 2016, Cell Reports *14*, 2624–2636
March 22, 2016
http://dx.doi.org/10.1016/j.celrep.2016.02.055

OPEN ACCESS
CellPress

Cell Reports
Article

The SNARE VAMP7 Regulates Exocytic Trafficking of Interleukin-12 in Dendritic Cells

Giulia Chiaruttini,[1] Giulia M. Piperno,[1] Mabel Jouve,[2] Francesca De Nardi,[1] Paola Larghi,[3,4] Andrew A. Peden,[5] Gabriele Baj,[6] Sabina Müller,[7] Salvatore Valitutti,[7] Thierry Galli,[8,9] and Federica Benvenuti[1,*]

[1]International Centre for Genetic Engineering and Biotechnology, Padriciano 99, 34149 Trieste, Italy
[2]Génétique et Biologie du Développement, UMR 3215, 26 rue d'Ulm, 75005 Paris, France
[3]Department of Pathophysiology and Transplantation, University of Milan, via F. Sforza 35, 20122 Milan, Italy
[4]Istituto Nazionale Genetica Molecolare "Romeo ed Enrica Invernizzi," via F. Sforza 35, 20122 Milan, Italy
[5]Centre for Membrane Interactions and Dynamics, Department of Biomedical Science, The University of Sheffield, Western Bank, Sheffield S10 2TN, UK
[6]Life Sciences Department, University of Trieste, via Giorgieri 5, 34127 Trieste, Italy
[7]Centre de Physiopathologie Toulouse-Purpan, Toulouse, INSERM UMR 1043, Toulouse 31300, France
[8]Institut Jacques Monod, UMR 7592, Centre National de la Recherche Scientifique, Université Paris Diderot, Sorbonne Paris Cité, 75013 Paris, France
[9]Membrane Traffic in Neuronal and Epithelial Morphogenesis, INSERM ERL U950, 75013 Paris, France
*Correspondence: benvenuti@icgeb.org
http://dx.doi.org/10.1016/j.celrep.2016.02.055

SUMMARY

Interleukin-12 (IL-12), produced by dendritic cells in response to activation, is central to pathogen eradication and tumor rejection. The trafficking pathways controlling spatial distribution and intracellular transport of IL-12 vesicles to the cell surface are still unknown. Here, we show that intracellular IL-12 localizes in late endocytic vesicles marked by the SNARE VAMP7. Dendritic cells (DCs) from VAMP7-deficient mice are partially impaired in the multidirectional release of IL-12. Upon encounter with antigen-specific T cells, IL-12-containing vesicles rapidly redistribute at the immune synapse and release IL-12 in a process entirely dependent on VAMP7 expression. Consistently, acquisition of effector functions is reduced in T cells stimulated by VAMP7-null DCs. These results provide insights into IL-12 intracellular trafficking pathways and show that VAMP7-mediated release of IL-12 at the immune synapse is a mechanism to transmit innate signals to T cells.

INTRODUCTION

The density of major histocompatibility complex (MHC)-peptide complexes (signal 1) and co-stimulatory molecules (signal 2) expressed on the surface of dendritic cells (DCs) is the main determinant of T cell activation during priming of adaptive immunity. Additional signals from pro-inflammatory cytokines (signal 3) secreted by DCs upon pathogen recognition have a profound impact in programming T cell fate by regulating early events of T cell receptor (TCR) signal transduction and by stabilizing gene expression in activated cells (Joffre et al., 2009). Interleukin-12 (IL-12), produced primarily by CD8α^+ DCs, is a key proinflammatory cytokine for CD4$^+$ Th1 differentiation and effector and memory CD8$^+$ T cell function (Curtsinger and Mescher, 2010; Moser and Murphy, 2000; Mashayekhi et al., 2011). Cytokine production is mostly regulated at the transcriptional level (Weinmann et al., 2001). In addition, it recently emerged that cytokine release is timely and spatially controlled by protein trafficking complexes (Herda et al., 2012; Stow et al., 2006). Vesicles of newly synthetized IL-12 in DCs become redistributed along microtubules and gather at the site of interaction with T or natural killer (NK) cells, the so-called immune synapse (IS) (Borg et al., 2004; Pulecio et al., 2010). Yet, the molecular machinery that controls transport of IL-12 from the site of production to the plasma membrane (PM) for multifocal or polarized release at the IS has not been unveiled.

The soluble N-ethylmaleimide-sensitive factor accessory protein receptor (SNARE) family of proteins constitutes the core machinery orchestrating intracellular membrane fusion events. Secretion of pre-stored granules in granulocytes and cytotoxic T cells depends on late endosomal SNAREs such as VAMP7, VAMP8, and VAMP2 (Mollinedo et al., 2006; Tiwari et al., 2008; Dressel et al., 2010; Krzewski et al., 2011; Matti et al., 2013). Release of soluble cytokines by immune cells is by far less understood. The present evidence indicates a role for VAMP3 and recycling endosomes in the release of tumor necrosis factor α (TNF-α) and IL-6 in macrophages and for interferon γ (IFN-γ) secretion in NK cells (Manderson et al., 2007; Reefman et al., 2010). An alternative secretory mechanism via early rather than recycling endosomes has recently been proposed for the secretion of IFN-γ by T cells (Herda et al., 2012).

Here, we show that intracellular IL-12 is contained in late endocytic compartments that stain positive for the SNARE VAMP7 and are recruited at the site of interaction with antigen specific T cells. Loss of VAMP7 partially inhibited the general,

multidirectional secretion of IL-12. Most importantly, VAMP7 deletion in DCs resulted in complete abrogation of the secretory peak that follows synapse formation and compromised differentiation of T cells into IFN-γ-producing cells. This represents an unusual pathway of cytokines trafficking via late endocytic compartments and unveils the mechanism used by DCs to transmit soluble signal 3 to T cells during initiation of adaptive immunity.

RESULTS

Subcellular Distribution of SNAREs in DCs

IL-12 is a heterodimeric cytokine composed of two subunits, p40 and p35, that dimerize to form biologically active IL-12/p70 (Carra et al., 2000). Stimulation of DCs with the TLR9 agonist CpG-B and, to a lesser extent, with the TLR4 agonist lipopolysaccharide (LPS) induces strong transcription of IL-12/p40 and a 10- to 15-fold increase in transcription of the p35 subunits within a few hours (Figure S1A). Protein secretion reflects gene expression, with a high secretory rate within 3 to 6 hr postinduction (Figure S1B).

To identify the machinery involved in IL-12 release, we focused on three SNAREs that classically mark different steps along the endocytic pathway. STX6 is a Q-SNARE involved in *trans*-Golgi network (TGN) to endosome trafficking; VAMP3 is a marker of early and recycling endosomes (Bajno et al., 2000; Manderson et al., 2007), and VAMP7 marks late endosomes and controls fusion of Golgi and late-endosomal compartments with the cell surface (Burgo et al., 2012; Danglot et al., 2012; Martinez-Arca et al., 2000; Ward et al., 2000). Their subcellular distribution in DCs was consistent with their localization in other cellular models (Figure 1A). STX6 was highly enriched in the Golgi and in cytoplasmic EEA-1$^+$ structures, poorly associated with recycling endosomes (Rab11), and excluded from late endosomes (CD63). VAMP3 was found in the Golgi and in peripheral vesicles that express EEA-1 and Rab11, but not in CD63-expressing vesicles. The vesicular SNARE VAMP7 showed a strong overlap with peripheral organelles stained with anti-CD63 and only little overlap with EEA-1 and Rab11 (Figure 1A). DC stimulation by bacterial agonist induced an increase in SNARE gene transcription and protein levels (Figures 1B and 1C). Thus, innate signals boost production of trafficking proteins concomitantly to the maximal peak of cytokine secretion.

Localization of Intracellular IL-12 in Endocytic Organelles

We next used different approaches and markers to investigate the intracellular distribution of IL-12 in DCs. Cells were stimulated with CpG-B for 3.5 hr, a time point at which the secretory rate is maximal and intracellular IL-12 (p40 subunit) is clearly detected by antibody staining. All SNAREs colocalized with IL-12 in the Golgi area, reflecting accumulation of newly synthesized protein (Figure 2A). In peripheral post-Golgi compartments, IL-12 p40 was associated with VAMP7 and only partially with VAMP3. Instead, it was almost entirely excluded from STX6-positive structures (Figure 2A). To detect bioactive IL-12/p70, for which no antibodies for immune labeling are available, we overexpressed a recombinant p35 protein fused to a small SV5 tag or to GFP. Recombinant p35 was secreted as heterodimer with endogenous p40 and largely co-distributed with the p40 subunit by immunostaining (Figures S2A–S2F). The p35 subunit displayed a consistent overlap with VAMP7 in the Golgi and in peripheral vesicles, whereas colocalization with VAMP3 was less pronounced (Figure 2B). VAMP7, p35, and p40 overlapped in several central and peripheral structures, indicating that the biologically active p70 heterodimer traffics via VAMP7 vesicles (Figure S2G). Intracellular Il-12 vesicles merged to structures positive for pHrodo-dextran, a conjugate that emits bright red fluorescent upon internalization into acidic compartments (Figure 2C). Furthermore, p35 was found to be highly associated with Rab7, a protein that selectively marks late endocytic vesicles (Chavrier et al., 1990; Gotthardt et al., 2002) (Figure 2D). We also found a consistent association of p35 with intracellular MHC class-II-positive compartments (Figure 2D), a peculiar class of tubular endosomes implicated in transport of MHC class II molecules from lysosomes to the cell surface during DCs maturation (Chow et al., 2002; Kleijmeer et al., 2001). Intriguingly, this association suggests that IL-12 may share, at least in part, its journey to the cell surface with vesicles carrying the MHC-II molecules.

To investigate IL-12 compartments at the ultra-structural level, we performed immunoelectron microscopy on cells expressing p35-SV5. A large part of labeling was found associated with Golgi stacks and in many nearby tubulovesicular membranes representing the TGN. A fraction of the protein was contained in vesicles and tubules associated with late-endosomes/lysosomes (arrowheads) (Figure 2E). These structures are morphologically similar to the ones described for MHC class II molecules in DCs (Barois et al., 2002).

Altogether, these results indicate that post-Golgi trafficking of bioactive IL-12 in DCs utilizes late endocytic vesicles preferentially marked by the SNARE VAMP7.

Loss of VAMP7 Inhibits IL-12 Secretion

To examine the function of VAMP7 during IL-12 release, we analyzed secretion in DCs derived from VAMP7 knockout mice (V7KO) (Danglot et al., 2010). Gene targeting resulted in complete loss of VAMP7 in DCs (Figure S3A). The frequency of CD11c$^+$/MHC-II^{high} conventional DCs and the percentage of CD8α$^+$ DCs, the main IL-12 producers, were normal in V7KO mice as compared to their wild-type (WT) littermates, indicating that VAMP7 is dispensable for DC development (Figures S3B and S3C). Secretion of the bioactive IL-12/p70 dimer was modestly but consistently reduced in V7KO cells as compared to controls, whereas IL-12/p40 secretion and IL-6 secretion were mostly unaffected (Figure 3A). Importantly, production of IL-12/p70 was consistently reduced in primary DCs isolated from the spleen of VAMP7-null mice (Figure 3B). In splenic DCs, IL-6 secretion was slightly affected by loss of VAMP7. Instead, the levels of TNF-α, a cytokine whose secretion depends on recycling endosomes and VAMP3 (Murray et al., 2005a), were not affected by VAMP7 deletion, indicating that different membrane trafficking routes are involved in the secretion of different cytokines. Phosphorylation of IKKα and β, ERK, and p38, was similar in WT and V7KO DCs, ruling out that decreased IL-12/p70 may depend on reduced TLR9 signaling (Figure S4A). Moreover, expression of maturation

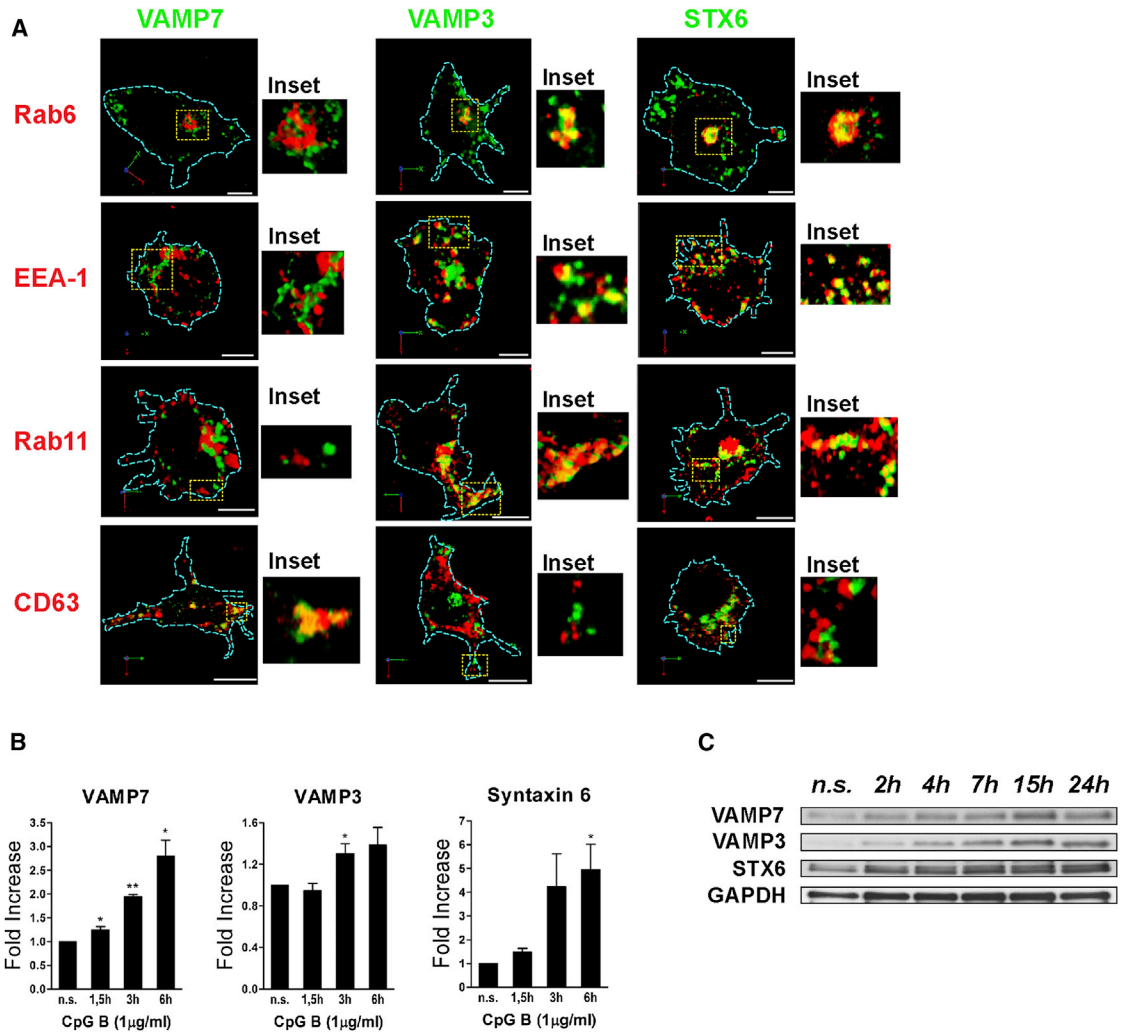

Figure 1. SNARE Localization in DCs

(A) SNARE distribution in DCs. Cells were co-stained with antibodies against endogenous VAMP7, VAMP3, and STX6 (green) and antibodies to Rab6, EEA-1, Rab11, and CD63 (red). GFP-VAMP3 was overexpressed to assess colocalization with Rab6 and Rab11. Images are representative 3D reconstructions of confocal z planes. Dashed lines define the cell boundaries. Insets are magnifications of the regions indicated by dashed lines. All scale bars in micrographs correspond to 5 μm.

(B) Fold increase of VAMP7, VAMP3, and STX6 mRNA expression in CpG-B-stimulated DCs. RT-PCR data were normalized to the housekeeping gene GAPDH. Bars show the mean ± SEM of three independent experiments. *$p < 0.05$ and **$p < 0,01$, Student's t test.

(C) Levels of SNARE proteins in resting (n.s.) and CpG-B-stimulated BM-DCs at different time points poststimulation. GAPDH was used as loading control.

markers (MHC-II and costimulatory molecules) and induction of cytokine gene transcription were comparable in the two genotypes (Figures S4B–S4D). To exclude cell-extrinsic contributions in DCs derived from V7KO mice, we knocked down VAMP7 expression in WT DCs (Figures S5A–S5D). The level of secreted IL-12/p70 was partially but reproducibly inhibited in DCs transfected with siVAMP7 as compared to control, whereas IL-12/p40 secretion was not affected (Figure 3C). We observed a certain degree of reduction in extracellular IL-6 too, suggesting that acute depletion of VAMP7 perturbs also the secretion of this cytokine. Induction of cytokine-coding mRNAs was unaffected by VAMP7 loss, ruling out an effect on cytokine-genes induction (Figure S5E). In sum, we conclude that loss of VAMP7 affects the general, multidirectional secretion of newly synthetized bioactive IL-12/p70.

Recruitment of SNARE and IL-12 at the Synapse

Global reorganization of the DCs subcellular space during the encounter with an antigen-specific T cell is important to promote T cell activation (Bloom et al., 2008; Pulecio et al., 2010). However, the trafficking proteins implicated in directional transport of vesicles to the DC immune synapse (DC-IS) have not been identified. To investigate the distribution of SNAREs during synapse formation, DCs were pulsed with ovalbumin (OVA) class I peptide and mixed with OVA-MHC class-I-specific $CD8^+$ T cells (OT-I) for different periods. As a control, we tracked distribution

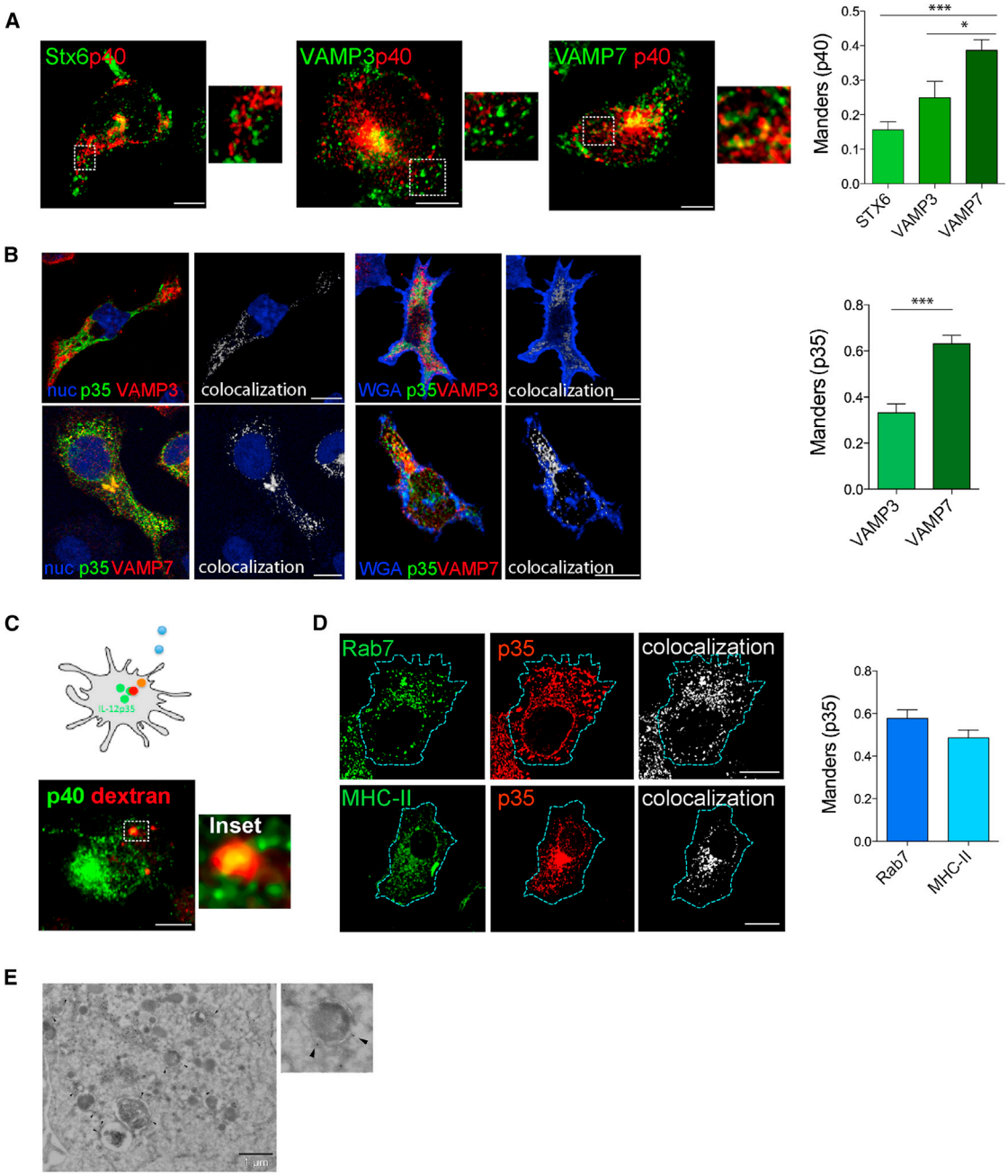

Figure 2. Bioactive IL-12 Localizes to Late Compartments Marked by VAMP7

(A) Representative medial confocal planes of DCs co-labeled with antibodies to p40 and to STX6, VAMP3, and VAMP7. Insets are magnifications of the post-Golgi regions indicated by dotted lines. Bars are Manders coefficients of p40 and the different SNAREs calculated on the whole-cell cytoplasm (excluding the Golgi region). Data are mean ± SEM. For each condition, at least 20 cells were analyzed in three independent experiments. *$p < 0.05$ and ***$p < 0.001$, Mann-Whitney t test.

(B) Distribution of the p35 bioactive subunit of IL-12. DCs expressing p35 were co-labeled for VAMP3 or VAMP7, nucleus or cell membrane (WGA). Representative confocal sections and co-localization channel for p35 and SNAREs are shown. Bars on the right show the Manders coefficient of p35 in the cell periphery. Mean ± SEM are plotted. For each condition, at least 20 cells were analyzed in three independent experiments. ***$p < 0.0001$, Mann-Whitney t test.

(C) Scheme of experimental design. DCs were loaded with pHrodo dextran (red) and stimulated with CpG-B, followed by labeling with anti-p40 antibodies (green). The inset highlights an intracellular structure where the two signals fully overlap.

(D) Localization of the p35 subunit with endosomal markers. WT DCs were transfected with p35-SV5 and labeled with anti-Rab7 and anti-SV5 antibodies. MHC-II GFP knockin DCs expressing p35-SV5 were labeled with antibodies to SV5 and to GFP. Single representative planes for each channel and the corresponding

(legend continued on next page)

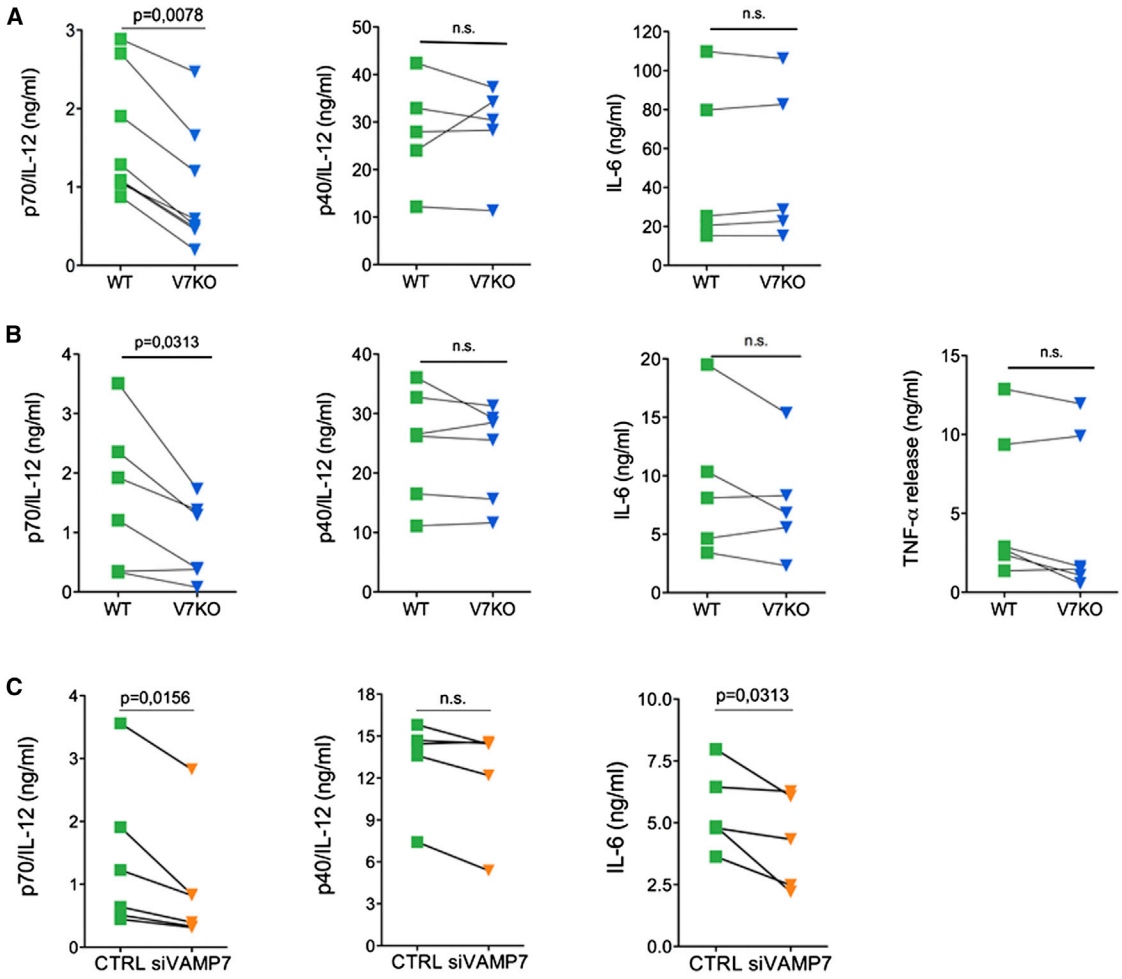

Figure 3. VAMP7 Deficiency in DCs Leads to Reduced Secretion of IL-12/p70

(A) DCs derived from the bone marrow of WT or V7KO mice were stimulated for 3 hr with CpG-B. Cytokine concentration in cell culture supernatants was quantified by ELISA.

(B) DCs were isolated from the spleen of WT or V7KO mice, stimulated for 6 hr with CpG-B and analyzed for cytokine secretion in cell culture supernatants. Each dataset refers to one independent experiment. p values were determined by Wilcoxon matched pairs test; n.s., not significant.

(C) Cytokine secretion in DCs expressing control (CTRL) or VAMP7-specific siRNA. Control and VAMP7-depleted cells were stimulated with CpG-B for 5 hr. The concentration of IL-12/p70, IL-12/p40, and IL-6 in cell culture supernatants was determined by ELISA. Each data point represents values from one independent experiment. p values were determined by Wilcoxon matched pairs test; n.s., not significant.

in antigen-nonspecific DC-T cell doublets. As early as 10 min after contact, the SNARE VAMP7 was found enriched at the DC-IS in a large proportion (up to 50%) of antigen-specific conjugates (as compared to a basal recruitment seen in 23% of nonspecific conjugates) (Figures 4A left and middle, and 4B). The same extent of polarization was maintained at later time points. VAMP3 was recruited in a similar proportion of antigen-specific conjugates, albeit with a slower kinetic. Polarization was similar in DCs expressing GFP-tagged SNAREs, thus excluding confounding effects from SNARE labeling in T cells (Figure 4A, right).

Trafficking of cytokines to specific PM regions such as the phagocytic cup in macrophages or the synapse in T cells is an important SNARE-mediated mechanism to confine delivery of soluble mediators (Huse et al., 2006; Murray et al., 2005a). Similarly to what we have found for the p40 subunit of IL-12 (Pulecio et al., 2010), p35 was polarized toward the synaptic interface in ~50% of DC-T antigen-specific doublets (data not shown). To identify the vesicles carrying IL-12 to the synaptic region, we measured colocalization indexes along 3D reconstructed synaptic interfaces. Several areas of overlap between p35 and VAMP7

colocalization mask are shown. The Manders coefficient for p35 and the two endosomal markers is shown on the right (n = 18 and 23, respectively). All bars in micrographs correspond to 5 μM.

(E) Ultrathin cryosections of DC expressing p35-SV5 immunogold-labeled for SV5. Solid arrowheads indicate labeling in tubules associated to late endosomes/lysosomes. The inset shows p35 labeling in the limiting membrane of a late endosomes.

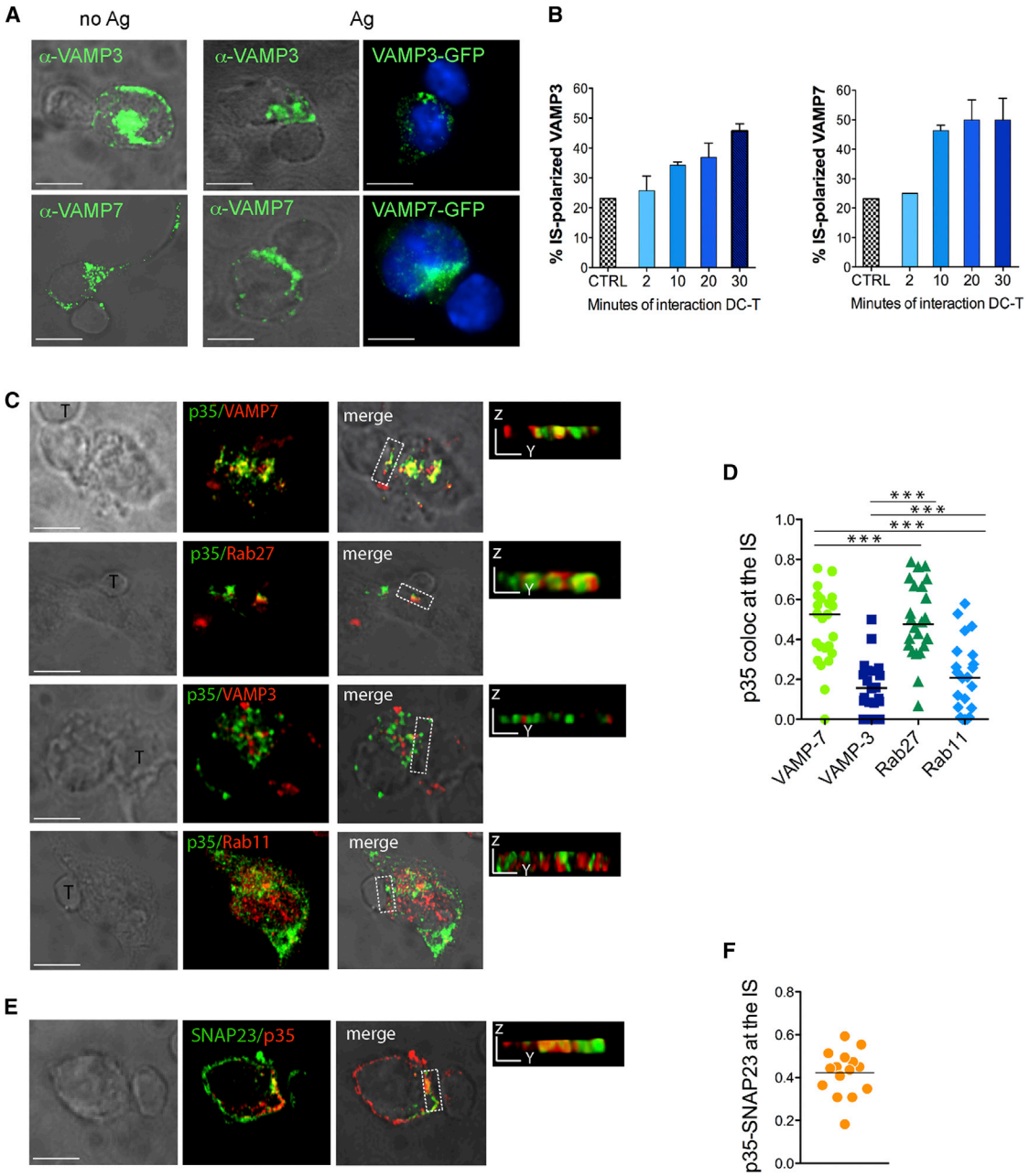

Figure 4. IL-12 Is Recruited at the Synapse in Late Endocytic Vesicles

(A) TLR-stimulated DCs were loaded (Ag) or not (no Ag) with OVA class-I peptide and mixed to OVA-specific $CD8^+$ T cells. Cells were fixed after 30 min and labeled with antibodies against endogenous VAMP7 and VAMP3.

(B) Kinetic of SNARE polarization. DC-T cell interaction was stopped by fixation at the indicated time points. Control (CTRL) refers to no antigen-conjugates stopped after 30 min. Bars show the percentage ± SEM of DCs with polarized SNARE. At least 30 conjugates per condition were analyzed in two independent experiments. The right panels show DCs overexpressing GFP-VAMP7 or GFP-VAMP3 mixed with T cells for 30 min.

(C) Analysis of localization of bioactive IL12/p70 vesicles at the synapse. DCs were transfected with p35-SV5 (or p35-GFP for VAMP7 staining) and mixed with T cells for 30 min. Fixed cells were labeled with antibodies to SV5 or GFP (green) and to VAMP7, VAMP3, Rab27a, or Rab11 (red). Representative confocal panels show fluorescent channels, DIC images, and the y-z 3D views of the synaptic region indicated by dashed boxes.

(D) The graph represents Pearson's correlation coefficient (PC) between p35 and the different organelle markers in the synaptic region (insets) calculated on 3D-reconstituted z sections. Each dot refers to a single cell, and horizontal bars indicate SEM. ***$p < 0{,}0001$, Mann-Whitney t test.

(E and F) DC-T conjugates (E) were labeled with antibodies against p35-SV5 and SNAP23. A representative example of the two proteins co-clustered at the IS is shown. The overlap between p35 and SNAP23 (F) was quantified in the synaptic area of 15 cells. All scale bars in micrographs correspond to 5 μm.

were present underneath the synaptic membrane, whereas the overlap with VAMP3 was less frequent (Figures 4C and 4D). Quantification of two other markers of the endocytic compartment (Rab11 for recycling endosomes and Rab27 for late endosomes/secretory granules) confirmed a preferential association between presynaptic p35 and late compartments (Figures 4C and 4D). Surface delivery of secretory proteins via vesicular SNARE requires a cognate PM acceptor complex constituted by the R-SNAREs SNAP23 and Syntaxin 4 in immune cells (Murray et al., 2005b; Pagan et al., 2003). Indeed, SNAP23 was found co-enriched with IL-12 at the synaptic membrane (Figures 4E and 4F), indicating a final SNARE-mediated step of exocytosis. Polarization of p35 at the DC-IS and association of the cytokine to late endosomal markers was confirmed in human DCs (Mo-DCs) (Figure S6).

Dynamics of VAMP7 and IL-12 Polarization at the IS

In order to gain a dynamic picture of polarization events occurring in DCs upon synapse formation and to resolve the kinetic of VAMP7 redistribution, we recorded DC-T cell interactions by time-lapse video microscopy. DCs expressing a VAMP7-RFP fusion protein (Burgo et al., 2012) were mixed with OT-I cells and immediately recorded to capture the first events upon encounter. As shown in still images extracted from Movie S1 (Figure 5A), VAMP7 clustered into large and bright structures upon a first T cell contact, as documented by a 1.7-fold increment in the total mean fluorescence intensity (MFI) of VAMP7-RFP (Figure 5B) that was maintained for over 25 min. The increase in fluorescence was paralleled by spatial redistribution of 80% of VAMP7 vesicles to the site of T cell contact (Figure 5C). Thus, synapse formation triggers a very rapid clustering and polarization of VAMP7 at the IS. Direct visualization of p35-GFP in DCs showed enrichment of the protein in a central perinuclear area and in fast-moving vesicles in the cell periphery. A particularly dynamic crowd of vesicles was observed underneath the membrane in contact with the T cell, as shown in the sequence in Figure 5D (extracted from Movie S2). Higher magnification of the synaptic zone evidenced tubulo-vesicular structures that dock and fuse with the synaptic PM (Figure 5D; Movie S3). Finally, in an effort to visualize events of p35 trafficking via VAMP7 vesicles at the IS, we co-expressed VAMP7-RFP and p35-GFP in DCs. Although the percentage of viable double-transfected cells was extremely low, we could detect an example of a double-positive vesicle appearing 10 min after contact and moving toward the synapse followed by signal decay at 20 min, suggesting its fusion with the membrane (Movie S4; Figure 5E).

VAMP7 Controls Synaptic Secretion and T Cell Priming

Clustering of IL-12/VAMP7$^+$ vesicles at DC-T contact suggests that VAMP7 may serve a specific and non-redundant function during polarized secretion at the synapse. To directly test this hypothesis, we set up an assay to measure secretion induced by T cell contact. Antigen-specific T cells were added to DCs that had been stimulated to reach the peak of intracellular IL-12 content. DCs and T cells were allowed to interact for as little as 10 min (in the presence or absence of cognate antigen), and the supernatant was harvested to measure IL-12 content. The values plotted in Figure 6A represent the sum of the cytokine accumulated in wells during 3.5 hr of stimulation (general secretion) plus the amount secreted during the 10 min of interaction with T cells (synapse-induced secretion). Co-culture of WT DCs with T cells in the presence of antigen (+Ag) induced a net increase in IL-12/p70 not seen in control wells without antigen. This indicates that antigen-specific interactions cause a secretory burst. This T cell-induced secretion was totally abrogated in V7KO DCs (Figure 6A, +Ag, V7KO columns). The lower basal levels of IL-12/p70 in V7KO wells compared to the WT (no Ag) reflects reduced general secretion. Thus, VAMP7 expression is required to release IL-12 in response to antigen specific synapse formation.

Analysis of the subcellular distribution of p35 vesicles in WT and VAMP7-null cells, using actin counterstaining to visualize cell boundaries, unveiled macroscopic differences in vesicles shape and position. In WT cells, p35 was found enriched all along the nuclear membrane and strongly accumulated in the Golgi. Multiple structures, both tubular and vesicular, were seen departing toward the cell periphery and intersecting the PM. Instead, p35 was condensed in larger structures retracted toward the nucleus in VAMP7-null cells with fewer single vesicles approaching the PM (Figure 6B). Quantification of the mean distance between cortical actin (PM) and p35 vesicles showed a significant increase in VAMP7-deficient cells, suggesting a slower transition from early biosynthetic compartments to carriers directed to the PM (Figure 6C).

To study the consequences of VAMP7 loss on T cell priming we pulsed WT or V7KO DCs with graded doses of OVA class I and mixed them with OT-I cells. The levels of IFN-γ secreted by CD8$^+$ T lymphocytes primed by V7KO DCs were significantly lower than those induced by WT DCs (Figure 6D). Similarly, IFN-γ secretion by CD4$^+$ T cells was inhibited (Figure 6E). However, T cell proliferation was equal, suggesting that VAMP7 expression in DCs regulates selectively acquisition of effector functions in T cells rather than proximal TCR triggering and proliferation.

Thus, we conclude that VAMP7 expression in DCs is required for IL-12/p70 secretion in response to synapse formation and consequently for T cell differentiation into IFN-γ-producing cells.

DISCUSSION

Secretion of soluble factors by immune cells is a key event to coordinate the immune response in time and space. Indeed, cells of the immune system have evolved peculiar secretory modes to cope with the need to release diverse mediators with different kinetics and in multiple directions. In this study, we show that the SNARE VAMP7 plays a pivotal role in regulating secretion of IL-12, a key cytokine released by DCs upon infection. We demonstrate that VAMP7 plays a dual role in IL-12 secretion. In individual DCs, its basic function is to regulate optimal exocytosis of biologically active IL12/p70 produced by inflammatory stimuli. The second essential role of VAMP7 is to control, non-redundantly, synaptic secretion of the cytokine during interaction with a cognate T cell, i.e., at the immune synapse.

Cytokine secretion, defined in the past as a classical constitutive pathway, emerged to be controlled by complex and regulated machineries that vary depending on the cell type and

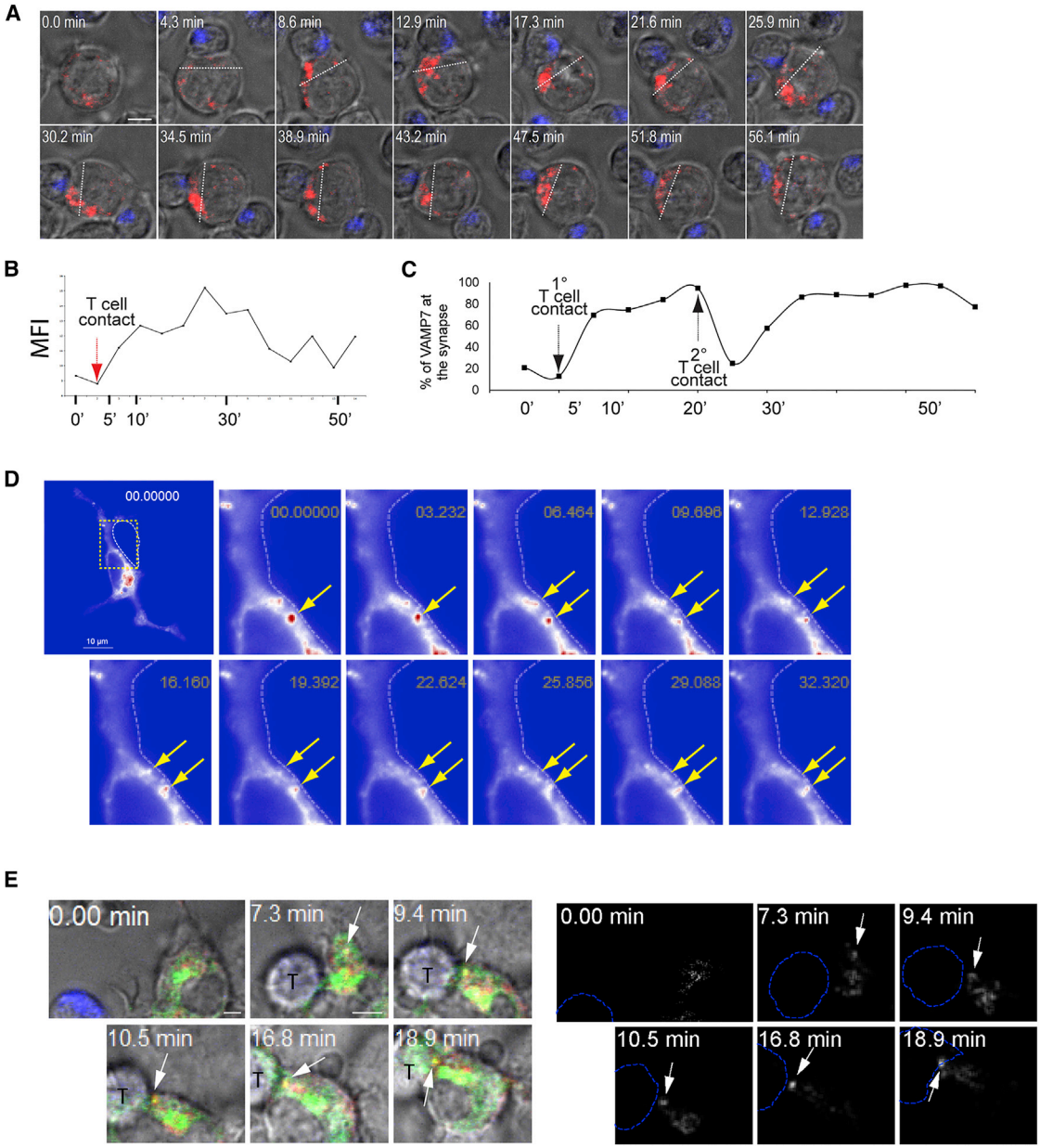

Figure 5. Dynamics of VAMP7 and IL-12 Polarization at the IS

(A) Time-lapse video microscopy snapshots showing VAMP7 distribution in DCs during synapse formation (Movie S1). DCs transfected with VAMP7-RFP were stimulated with CpG-B, pulsed with OVA class I peptide and mixed with OT-I cells (stained with membrane dye Bodipy 630, blue). Dashed lines define the DC's portion (one-third of the total cell) in contact with the T cell.

(B) The graph shows the mean fluorescence intensity (MFI) of RFP over time, before and after a T cell contact (arrow).

(C) Percentage of recruitment of VAMP7-RFP in the T cell proximal DC's portion over time. "1° T cell contact" indicates the time of synapse formation, and "2° T cell contact" indicates the formation of a collateral conjugate with a second T cell.

(D) DCs were transfected with p35-GFP and mixed with T cells. Images extracted from Movie S2 show peaks of green fluorescent signal (red pseudo-color indicated by yellow arrowheads) underneath the synaptic membrane (the T cell position is indicated by a dotted line).

(E) DCs were double-transfected with p35-GFP (green) and VAMP7-RFP (red), and mixed with OT-I cells (blue). Panels show representative frames extracted from a 30-min movie (Movie S4) and on the right the same sequence with a green and red colocalization channels (white). White arrows highlight a double-positive vesicle moving to the synapse and disappearing. All scale bars represent 5 μM.

context. In macrophages, TNF-α and IL-6 are trafficked via recycling compartments prior to be delivered at the cell surface (Murray et al., 2005b). Similarly, IFN-γ in NK cells (Reefman et al., 2010) and TNF in microglia cells (Hulse et al., 2008) transit through recycling endosomes whereas IFN-γ exocytosis in T cells is mediated by a yet unidentified compartment distinct

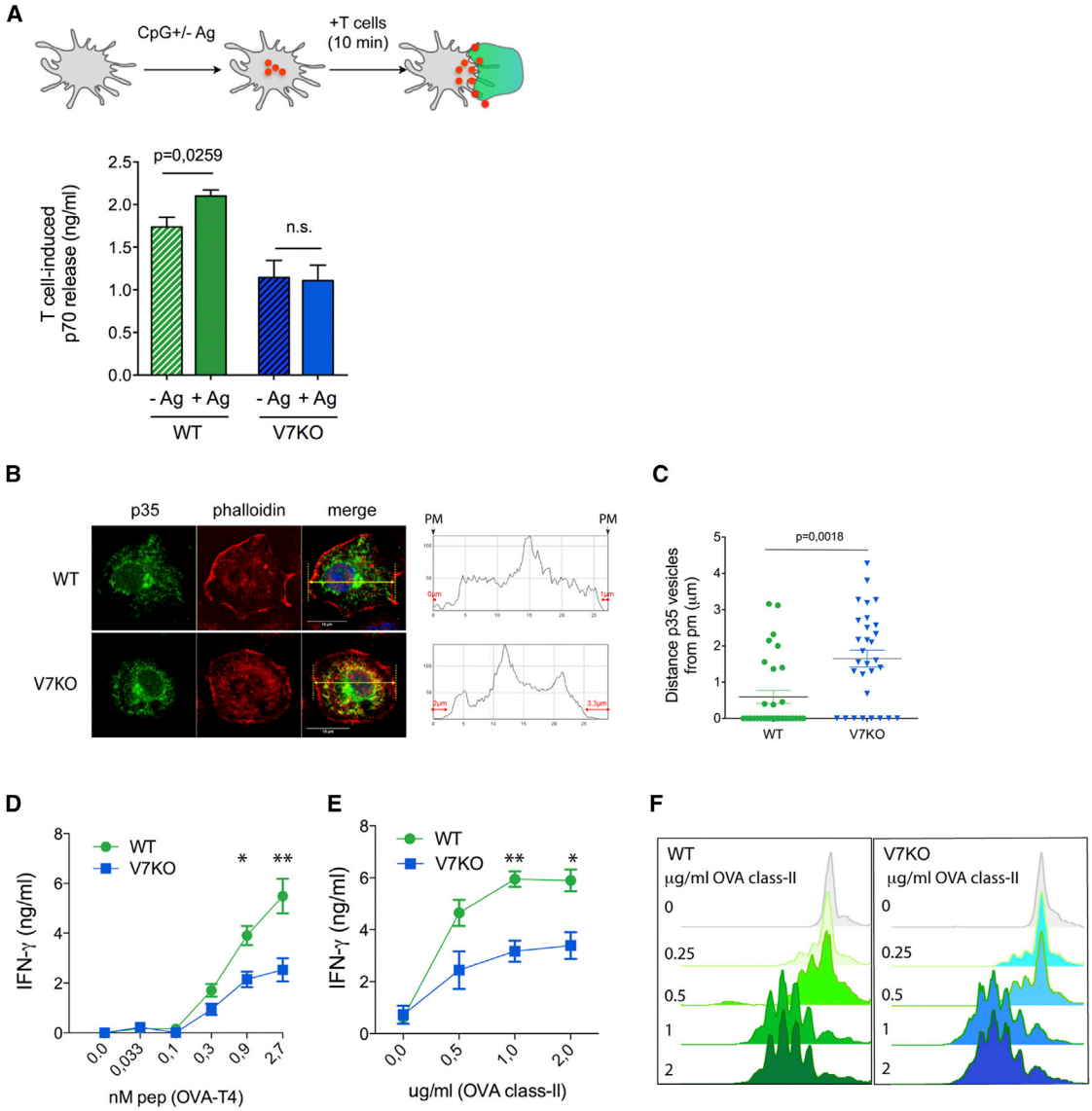

Figure 6. VAMP7 Expression in DCs Is Required for T Cell-Induced Secretion and T Cell Differentiation

(A) Synapse-induced secretion of IL-12/p70. Scheme of the experimental design: WT and V7KO DCs were stimulated with CpG-B and pulsed or not with OVA class I peptide. After 3 hr, naive $CD8^+$ OT-I cells were added to all wells and spun for 1 min at 800 rpm to force interaction. Cell culture supernatants were collected after 10 min of co-incubation at 37°C. Plotted are the values of IL-12/p70 in DC-T wells containing (+Ag) or not (−Ag) the antigen. Shown are the mean ± SEM of seven independent experiments. p values were determined by Student's t test.

(B) Distribution of p35-SV5 in WT and V7KO cells. Medial confocal optical sections of cells labeled to detect p35 and actin (phalloidin). A region (arrows in merge) was depicted to define cell boundaries. The mean distance of the most peripheral p35 vesicles from the plasma membrane (PM) is shown on the right. Red lines indicate the distances of p35 from each side of the cell.

(C) Dots in the graph correspond to the mean distance of p35 from the membrane, calculated in individual cells. Zero values indicate that p35 overlapped the membrane in at least one point. Horizontal bars indicate mean ± SEM. p values were determined by Mann-Whitney t test.

(D) $CD8^+$ T cell priming by WT and V7KO DCs. DCs were loaded with graded doses of low-affinity OVA class I peptide (T4) and mixed with $CD8^+$ OT-I cells for 48 hr. IFN-γ content in cell culture supernatant was evaluated by ELISA. Results are the mean ± SEM of three independent experiments.

(E) WT and V7KO DCs were stimulated with CpG-B and different doses of OVA class II peptide and then washed and co-cultured with $CD4^+$ OT-II cells for 72 hr.

(E and F) The IFN-γ level (E) and the CFSE dilution profile (F) are shown. Data are mean ± SEM of three independent experiments. *$p < 0.05$ and **$p < 0.01$, Student's t test.

from recycling endosomes (Herda et al., 2012). Cytokines trafficking in DCs has only begun to be addressed very recently (Collins et al., 2014). Ligation of Toll-like receptors (TLRs) by pathogen-derived molecules triggers massive cytokines biosynthesis and release in the few hours that follow stimulation. Interestingly, the peak in IL-12 gene transcription coincided to

upregulation of STX6 and VAMP7, demonstrating that DCs selectively adapt their trafficking machinery to sustain the intense post-infection secretory rate. Co-regulation of cytokine and exocytic machinery has been previously demonstrated in macrophages, where LPS induces the upregulation of STX6, Vti1b, and VAMP3 (Murray et al., 2005a, 2005b), concomitantly with the peak in TNF-α secretion.

By confocal and ultrastructural analysis, we found that post-Golgi trafficking of the p35 subunit of IL-12 involves transit via vesicles associated to late endosomes. Comparative analysis of co-localization with different SNAREs to identify regulatory proteins potentially involved in IL-12 transport revealed a preferential association with VAMP7-positive vesicles. Moreover, intracellular IL-12 overlapped with Rab7, strongly indicating that the protein is associated with late endosomes and, likely, secretory lysosomes (Daniele et al., 2011). The fact that the overlap with late endosomal markers is restricted to few vesicular structures/cell probably reflects a rapid transit of the protein through this station.

Protein knockdown experiments and genetic deletion confirmed a role for VAMP7 in controlling bioactive IL-12 release. Importantly, we showed, using multiple approaches, that VAMP7 depletion affects selectively cytokine exocytosis, as none of the upstream events such as TLR9 signaling, DCs maturation, and cytokine gene transcription were affected by VAMP7 deficiency. Inhibition of secretion was only partial, although reproducible over many experiments and it was similar in acute (small interfering RNA) and constitutive (knockout mice) models of depletion.

Interestingly, we observed a selective reduction of the IL-12/p70 isoform of IL-12. Secretion of the p70 (p35 + p40) heterodimer is regulated by post-translational modifications of the p35 subunit, including glycosylation and sequential cleavage steps of the leader peptide (Carra et al., 2000; Murphy et al., 2000). Thus, it is interesting to speculate that trafficking via VAMP7 may be required to undergo the full spectra of post-translational modification necessary for secretion.

The major and exclusive role of VAMP7 in DCs became apparent when examining a specific mode of IL-12 secretion, i.e., the one induced by a contact with a cognate antigen-specific T cell. The exquisite function of DCs is to activate naive T cells by providing information about the type of antigen (MHC-peptide complexes) and the environment (costimulatory molecules and cytokines). This informational transfer occurs in specialized DC-T cell junctions, and it is accompanied by active remodeling of the actin and microtubule cytoskeleton and by directional delivery of MHC class II complexes at the surface of the interaction (Al-Alwan et al., 2003; Boes et al., 2002; Chow et al., 2002; Pulecio et al., 2010; Comrie et al., 2015). Here, we uncover part of the machinery involved in directional trafficking and polarized release. Using fixed and live-cell imaging, we found that synapse formation causes recruitment of two vesicular SNAREs, VAMP3 and VAMP7, at the contact region. This finding by itself strongly reinforces the notion that DCs, similarly to what has been extensively documented in T cells (Bertrand et al., 2010; Das et al., 2004; Depoil et al., 2005; Huse et al., 2006), reorient vesicular flow during synapse formation. Detailed analysis of the synaptic interface showed that VAMP7$^+$ IL-12/p70 carriers accumulate at the IS. Time-lapse movies of DCs expressing p35-GFP revealed an intense trafficking of vesicles throughout the cell periphery that is more intense in the sites of contact with T cells, where GFP$^+$ tubulovesicular structures accumulate and fuse with the PM. Analysis of DC lines, even if less physiological, will be used in the future to better document in live the journey of p35-GFP to the membrane and its actual exocytosis at the IS.

The finding that VAMP7 depletion completely abrogated the burst in IL-12/p70 release induced by T cells strongly supports a selective and exclusive role of this membrane fusion protein in controlling confined delivery of IL-12 in *cis*, i.e., to the interacting antigen-specific T cell.

The pathway of IL-12 secretion that we have discovered is unusual for cytokines and bears analogies with pathways classically involved in regulated secretion. VAMP7 controls endo-lysosomal fusion and TGN to late endosome transport (Advani et al., 1999; Chaineau et al., 2009; Pols et al., 2013), and it has been implicated in exocytosis of pre-stored mediators from secretory lysosomes (Krzewski et al., 2011; Puri et al., 2003). Is this unique trafficking pathway specific for IL-12, or is it a specialization developed by DCs? The heterodimeric structure of IL-12 is atypical among cytokines, which may in part explain this peculiar route of secretion. Second, DCs have evolved unique modifications of their endocytic pathway for the sake of optimal antigen uptake and processing (Gatti and Pierre, 2003). These include the usage of endo-lysosomal compartments such as multivesicular bodies (MVBs) as a TLR-inducible pathway to deliver MHC class II molecules at the cell surface in a polarized fashion (Boes et al., 2003; Kleijmeer et al., 2001). Indeed, MVBs were recently shown to be regulated by VAMP7 (Fader et al., 2009). The presence of intracellular structures staining positive for IL-12 and MHC class II strongly suggests a joined traffic of antigen and cytokine at the synapse, a mechanism that would allow spatiotemporal synchronization in delivering different DC-derived signals to T cells.

The ultimate consequence of lack of VAMP7 in DCs is defective activation of IFN-γ secretion in T cells, a function that relies on IL-12-dependent signals and that is key for effector T cell function. Thus, VAMP7-mediated release represents a mechanism to confine ''soluble'' information to the antigen-specific interacting T cell, thereby conditioning its fate.

Together, these findings provide a basis to understand the molecular machinery involved in secretion of IL-12 by DCs, a central process in initiation of adaptive immunity. It also highlights an unusual method of cytokine exit through late endocytic compartments, and it assigns a further key function to the SNARE VAMP7 in immune cell regulation.

EXPERIMENTAL PROCEDURES

Antibodies and Plasmids

VAMP3-GFP and VAMP7-GFP plasmids were a kind gift of Jennifer L. Stow (University of Queensland, Brisbane, Australia). P35-SV5 was cloned as described in Supplemental Experimental Procedures. VAMP7-RFP was described in Burgo et al. (2012). Antibodies against VAMP7 and VAMP3 were made in-house by Andrew A. Peden. All commercial antibodies are described in Supplemental Experimental Procedures.

Mice

VAMP7-deficient mice were described previously (Danglot et al., 2012). Male V7KO mice on a C57BL/6 background were compared with their male wild-type littermates. Mice were bred and maintained in sterile isolators. OVA-specific, MHC class I and MHC class II restricted, TCR transgenic Rag$^{-/-}$ OT-I and OT-II mice were purchased from the Jackson ImmunoResearch Laboratories. Bone marrow from I-A^{b} GFP mice (Boes et al., 2002) were a kind gift of Ana-Maria Lennon Dumenil (Insitut Curie, Paris, France). Animal care and treatment were conducted in conformity with institutional guidelines in compliance with national and international laws and policies (European Economic Community [EEC] Council Directive 86/609; OJL 358; December 12, 1987). Protocols were approved by the Italian Ministry of Health.

DC Culture and Transfections

DCs were differentiated from the bone marrow using FLT3L and depleted of B220^{+} cells for experiments. DCs were activated with CpG-B (1 μg/ml) for 3–4 hr to stain intracellular cytokines and for 3–6 hr to measure cytokine secretion. Splenic DCs were enriched from total spleen cells by positive selection using CD11c^{+} microbeads (Miltenyi Biotec). To express GFP-SNARE and p35-SV5, cells were transfected by nucleofection and used for experiments 3–4 hr after transfection. For siRNA experiments, cells were transfected by nucleofection and collected for experiments 48 hr later. Human DCs were generated from CD14^{+} monocytes isolated from peripheral blood mononuclear cells of healthy donors using Mo-DC differentiation medium (Miltenyi) for 7 days to generate immature Mo-DCs.

Immunofluorescence, Synapse Formation, and Confocal Analysis

DCs were stimulated with CpG-B for 3-4 hr to induce accumulation of intracellular IL-12. Cells were fixed (4% paraformaldehyde), permeabilized (PBS/BSA 0.2%/saponin 0.05%), and immunolabeled with antibodies against the different endosomal markers (as described in Supplemental Experimental Procedures) or tags (SV5 or GFP). To visualize IL-12 in endocytic vesicles, PHrodo red dextran (Molecular Probes) was given to cells (100 μg/ml) together with CpG-B stimulation. For synapse formation, DCs were stimulated with CpG-B and pulsed with class I or class II OVA peptide and adhered to fibronectin-coated slides. OT-I or OT-II cells were added to DCs in a 1:1 ratio and incubated at 37°C for 30 min. Mo-DCs were loaded with 1 μg/ml superantigens (SEB and TSST1) and mixed with CD3/CD28 activated CD4^{+} T cells from the same donor. Cells were fixed and labeled with antibodies as indicated in Supplemental Experimental Procedures. Confocal z stacks of isolated DCs or synapses were acquired using a LSM510 META Axiovert 200M Image. Analysis of co-localization coefficients on 3D volumes were performed using Volocity 3D Image Analysis Software (Perkin Elmer) and ImageJ (NIH). For the colocalization mask in Figures 2B and 2E, the pixels containing both stainings above the threshold were used to generate a white channel. To quantify SNARE polarization, confocal z stack images were reconstructed and the SNARE was scored as polarized when the ratio between the MFI at the T cell contact zone and the MFI of the total DC PM was > 1. The distance of p35 vesicles form the membrane in WT and V7KO cells was measured on 3D-reconstructed volumes using ImageJ.

In Vivo Imaging

DCs expressing VAMP7-RFP or p35-GFP were layered on videomicroscopy chambers and recorder immediately after the addition of T cells. Time-lapse movies were acquired with a LSM510 META reverse microscope (Movies S1 and S4) or an Axio Observer.Z1 microscope. Videos were analyzed using ImageJ software.

T Cell-Induced Secretion Assay and T Cell Activation

2 × 10^{5} WT or V7KO BM-DCs were stimulated for 3 hr with CpG-B (1 μg/ml) and pulsed or not pulsed with 10 nM OVA I peptide. After stimulation, 9 × 10^{5} CD8^{+} OT-I cells were added to each well and spun down to force conjugate formation. After 10 min at 37°C, cells were pelleted and supernatants were collected to measure IL-12/p70 concentration. For T cell priming, 2 × 10^{4} WT and V7KO BM-DCs were stimulated and pulsed with graded doses of OVA class I (low-affinity T4 peptide) or class II peptide and then washed and mixed with 10^{5} OT-I cells for 48 hr or OT-II cells for 72 hr, respectively. In Figures 2E and 2F, OT-II cells were pre-labeled with 2 μM carboxyfluorescein succinimidyl ester (CFSE) before being added to DC wells. Cell culture supernatants were collected, and IFN-γ concentration was quantified.

Electron Microscopy

Immunoelectron microscopy was performed using the Tokuyasu method. Ultrathin cryosections were single or double labeled with antibodies against p35 and protein A-gold (PAG; Utrecht University, the Netherlands). Control labelings with anti-SV5 antibodies on nontransfected cells and with secondary antibodies alone were negative.

Statistical Analysis

All statistical analyses were performed using GraphPad Prism. The error bars show the SEM between mean values of independent experiments (as in the functional analyses and SNARE polarization analyses) or between values of single cells analyzed (SNARE/p35 co-localization at the IS and p35 distance from the PM). p values were obtained by Student's, Wilcoxon paired nonparametric, or Mann-Whitney t tests.

SUPPLEMENTAL INFORMATION

Supplemental Information includes Supplemental Experimental Procedures, six figures, and four movies and can be found with this article online at http://dx.doi.org/10.1016/j.celrep.2016.02.055.

AUTHOR CONTRIBUTIONS

F.B. designed experiments and wrote the paper. G.C. performed experiments and prepared figures. G.M.P. and F.D.N. performed experiments. M.J. performed immunoelectron microscopy analysis. P.L., A.A.P., and T.G. provided reagents and animal models. G.B., S.M., and S.V. provided support for imaging experiments.

ACKNOWLEDGMENTS

The work was funded by grants IG9076 and IG2013 14414 from the Associazione Italiana Ricerca Cancro and by grant 14-0320 from Worldwide Cancer Research (to F.B.). G.C. was supported by the AIRC, an ICGEB pre-doctoral fellowship, and an EMBO short term-fellowship. G.M.P. was supported by Telethon grant GGP14281. T.G. was supported by Agence Nationale de la Recherche (ANR-13-BSV2-0018-02) and Fondation ARC. M.J. was supported by the French National Research Agency through the "Investments for the Future" program (France-BioImaging, ANR-10-INSB-04). We thank Jennifer L. Stow for providing SNARE-GFP plasmids, Ana-Maria Lennon Dumenil and Danielle Lankar for providing I-Ab-GFP BM, Matteo Bellone and Matteo Grioni for providing OT-I cells on a Rag$^{-/-}$ background, and Ana-Maria Lennon Dumenil and Claire Hivroz for helpful discussions.

Received: September 23, 2015
Revised: December 21, 2015
Accepted: February 9, 2016
Published: March 10, 2016

REFERENCES

Advani, R.J., Yang, B., Prekeris, R., Lee, K.C., Klumperman, J., and Scheller, R.H. (1999). VAMP-7 mediates vesicular transport from endosomes to lysosomes. J. Cell Biol. *146*, 765–776.

Al-Alwan, M.M., Liwski, R.S., Haeryfar, S.M., Baldridge, W.H., Hoskin, D.W., Rowden, G., and West, K.A. (2003). Cutting edge: dendritic cell actin cytoskeletal polarization during immunological synapse formation is highly antigen-dependent. J. Immunol. *171*, 4479–4483.

Bajno, L., Peng, X.R., Schreiber, A.D., Moore, H.P., Trimble, W.S., and Grinstein, S. (2000). Focal exocytosis of VAMP3-containing vesicles at sites of phagosome formation. J. Cell Biol. *149*, 697–706.

Barois, N., de Saint-Vis, B., Lebecque, S., Geuze, H.J., and Kleijmeer, M.J. (2002). MHC class II compartments in human dendritic cells undergo profound structural changes upon activation. Traffic *3*, 894–905.

Bertrand, F., Esquerré, M., Petit, A.E., Rodrigues, M., Duchez, S., Delon, J., and Valitutti, S. (2010). Activation of the ancestral polarity regulator protein kinase C zeta at the immunological synapse drives polarization of Th cell secretory machinery toward APCs. J. Immunol. *185*, 2887–2894.

Bloom, O., Unternaehrer, J.J., Jiang, A., Shin, J.S., Delamarre, L., Allen, P., and Mellman, I. (2008). Spinophilin participates in information transfer at immunological synapses. J. Cell Biol. *181*, 203–211.

Boes, M., Cerny, J., Massol, R., Op den Brouw, M., Kirchhausen, T., Chen, J., and Ploegh, H.L. (2002). T-cell engagement of dendritic cells rapidly rearranges MHC class II transport. Nature *418*, 983–988.

Boes, M., Bertho, N., Cerny, J., Op den Brouw, M., Kirchhausen, T., and Ploegh, H. (2003). T cells induce extended class II MHC compartments in dendritic cells in a Toll-like receptor-dependent manner. J. Immunol. *171*, 4081–4088.

Borg, C., Jalil, A., Laderach, D., Maruyama, K., Wakasugi, H., Charrier, S., Ryffel, B., Cambi, A., Figdor, C., Vainchenker, W., et al. (2004). NK cell activation by dendritic cells (DCs) requires the formation of a synapse leading to IL-12 polarization in DCs. Blood *104*, 3267–3275.

Burgo, A., Proux-Gillardeaux, V., Sotirakis, E., Bun, P., Casano, A., Verraes, A., Liem, R.K., Formstecher, E., Coppey-Moisan, M., and Galli, T. (2012). A molecular network for the transport of the TI-VAMP/VAMP7 vesicles from cell center to periphery. Dev. Cell *23*, 166–180.

Carra, G., Gerosa, F., and Trinchieri, G. (2000). Biosynthesis and posttranslational regulation of human IL-12. J. Immunol. *164*, 4752–4761.

Chaineau, M., Danglot, L., and Galli, T. (2009). Multiple roles of the vesicular-SNARE TI-VAMP in post-Golgi and endosomal trafficking. FEBS Lett. *583*, 3817–3826.

Chavrier, P., Parton, R.G., Hauri, H.P., Simons, K., and Zerial, M. (1990). Localization of low molecular weight GTP binding proteins to exocytic and endocytic compartments. Cell *62*, 317–329.

Chow, A., Toomre, D., Garrett, W., and Mellman, I. (2002). Dendritic cell maturation triggers retrograde MHC class II transport from lysosomes to the plasma membrane. Nature *418*, 988–994.

Collins, L.E., DeCourcey, J., Rochfort, K.D., Kristek, M., and Loscher, C.E. (2014). A role for syntaxin 3 in the secretion of IL-6 from dendritic cells following activation of toll-like receptors. Front. Immunol. *5*, 691.

Comrie, W.A., Li, S., Boyle, S., and Burkhardt, J.K. (2015). The dendritic cell cytoskeleton promotes T cell adhesion and activation by constraining ICAM-1 mobility. J. Cell Biol. *208*, 457–473.

Curtsinger, J.M., and Mescher, M.F. (2010). Inflammatory cytokines as a third signal for T cell activation. Curr. Opin. Immunol. *22*, 333–340.

Danglot, L., Chaineau, M., Dahan, M., Gendron, M.C., Boggetto, N., Perez, F., and Galli, T. (2010). Role of TI-VAMP and CD82 in EGFR cell-surface dynamics and signaling. J. Cell Sci. *123*, 723–735.

Danglot, L., Zylbersztejn, K., Petkovic, M., Gauberti, M., Meziane, H., Combe, R., Champy, M.F., Birling, M.C., Pavlovic, G., Bizot, J.C., et al. (2012). Absence of TI-VAMP/Vamp7 leads to increased anxiety in mice. J. Neurosci. *32*, 1962–1968.

Daniele, T., Hackmann, Y., Ritter, A.T., Wenham, M., Booth, S., Bossi, G., Schintler, M., Auer-Grumbach, M., and Griffiths, G.M. (2011). A role for Rab7 in the movement of secretory granules in cytotoxic T lymphocytes. Traffic *12*, 902–911.

Das, V., Nal, B., Dujeancourt, A., Thoulouze, M.I., Galli, T., Roux, P., Dautry-Varsat, A., and Alcover, A. (2004). Activation-induced polarized recycling targets T cell antigen receptors to the immunological synapse; involvement of SNARE complexes. Immunity *20*, 577–588.

Depoil, D., Zaru, R., Guiraud, M., Chauveau, A., Harriague, J., Bismuth, G., Utzny, C., Müller, S., and Valitutti, S. (2005). Immunological synapses are versatile structures enabling selective T cell polarization. Immunity *22*, 185–194.

Dressel, R., Elsner, L., Novota, P., Kanwar, N., and Fischer von Mollard, G. (2010). The exocytosis of lytic granules is impaired in Vti1b- or Vamp8-deficient CTL leading to a reduced cytotoxic activity following antigen-specific activation. J. Immunol. *185*, 1005–1014.

Fader, C.M., Sánchez, D.G., Mestre, M.B., and Colombo, M.I. (2009). TI-VAMP/VAMP7 and VAMP3/cellubrevin: two v-SNARE proteins involved in specific steps of the autophagy/multivesicular body pathways. Biochim. Biophys. Acta *1793*, 1901–1916.

Gatti, E., and Pierre, P. (2003). Understanding the cell biology of antigen presentation: the dendritic cell contribution. Curr. Opin. Cell Biol. *15*, 468–473.

Gotthardt, D., Warnatz, H.J., Henschel, O., Brückert, F., Schleicher, M., and Soldati, T. (2002). High-resolution dissection of phagosome maturation reveals distinct membrane trafficking phases. Mol. Biol. Cell *13*, 3508–3520.

Herda, S., Raczkowski, F., Mittrücker, H.W., Willimsky, G., Gerlach, K., Kühl, A.A., Breiderhoff, T., Willnow, T.E., Dörken, B., Höpken, U.E., and Rehm, A. (2012). The sorting receptor Sortilin exhibits a dual function in exocytic trafficking of interferon-γ and granzyme A in T cells. Immunity *37*, 854–866.

Hulse, R.E., Swenson, W.G., Kunkler, P.E., White, D.M., and Kraig, R.P. (2008). Monomeric IgG is neuroprotective via enhancing microglial recycling endocytosis and TNF-alpha. J. Neurosci. *28*, 12199–12211.

Huse, M., Lillemeier, B.F., Kuhns, M.S., Chen, D.S., and Davis, M.M. (2006). T cells use two directionally distinct pathways for cytokine secretion. Nat. Immunol. *7*, 247–255.

Joffre, O., Nolte, M.A., Spörri, R., and Reis e Sousa, C. (2009). Inflammatory signals in dendritic cell activation and the induction of adaptive immunity. Immunol. Rev. *227*, 234–247.

Kleijmeer, M., Ramm, G., Schuurhuis, D., Griffith, J., Rescigno, M., Ricciardi-Castagnoli, P., Rudensky, A.Y., Ossendorp, F., Melief, C.J., Stoorvogel, W., and Geuze, H.J. (2001). Reorganization of multivesicular bodies regulates MHC class II antigen presentation by dendritic cells. J. Cell Biol. *155*, 53–63.

Krzewski, K., Gil-Krzewska, A., Watts, J., Stern, J.N., and Strominger, J.L. (2011). VAMP4- and VAMP7-expressing vesicles are both required for cytotoxic granule exocytosis in NK cells. Eur. J. Immunol. *41*, 3323–3329.

Manderson, A.P., Kay, J.G., Hammond, L.A., Brown, D.L., and Stow, J.L. (2007). Subcompartments of the macrophage recycling endosome direct the differential secretion of IL-6 and TNFalpha. J. Cell Biol. *178*, 57–69.

Martinez-Arca, S., Alberts, P., Zahraoui, A., Louvard, D., and Galli, T. (2000). Role of tetanus neurotoxin insensitive vesicle-associated membrane protein (TI-VAMP) in vesicular transport mediating neurite outgrowth. J. Cell Biol. *149*, 889–900.

Mashayekhi, M., Sandau, M.M., Dunay, I.R., Frickel, E.M., Khan, A., Goldszmid, R.S., Sher, A., Ploegh, H.L., Murphy, T.L., Sibley, L.D., and Murphy, K.M. (2011). CD8α(+) dendritic cells are the critical source of interleukin-12 that controls acute infection by Toxoplasma gondii tachyzoites. Immunity *35*, 249–259.

Matti, U., Pattu, V., Halimani, M., Schirra, C., Krause, E., Liu, Y., Weins, L., Chang, H.F., Guzman, R., Olausson, J., et al. (2013). Synaptobrevin2 is the v-SNARE required for cytotoxic T-lymphocyte lytic granule fusion. Nat. Commun. *4*, 1439.

Mollinedo, F., Calafat, J., Janssen, H., Martín-Martín, B., Canchado, J., Nabokina, S.M., and Gajate, C. (2006). Combinatorial SNARE complexes modulate the secretion of cytoplasmic granules in human neutrophils. J. Immunol. *177*, 2831–2841.

Moser, M., and Murphy, K.M. (2000). Dendritic cell regulation of TH1-TH2 development. Nat. Immunol. *1*, 199–205.

Murphy, F.J., Hayes, M.P., and Burd, P.R. (2000). Disparate intracellular processing of human IL-12 preprotein subunits: atypical processing of the P35 signal peptide. J. Immunol. *164*, 839–847.

Murray, R.Z., Kay, J.G., Sangermani, D.G., and Stow, J.L. (2005a). A role for the phagosome in cytokine secretion. Science *310*, 1492–1495.

Murray, R.Z., Wylie, F.G., Khromykh, T., Hume, D.A., and Stow, J.L. (2005b). Syntaxin 6 and Vti1b form a novel SNARE complex, which is up-regulated in

activated macrophages to facilitate exocytosis of tumor necrosis Factor-alpha. J. Biol. Chem. *280*, 10478–10483.

Pagan, J.K., Wylie, F.G., Joseph, S., Widberg, C., Bryant, N.J., James, D.E., and Stow, J.L. (2003). The t-SNARE syntaxin 4 is regulated during macrophage activation to function in membrane traffic and cytokine secretion. Curr. Biol. *13*, 156–160.

Pols, M.S., van Meel, E., Oorschot, V., ten Brink, C., Fukuda, M., Swetha, M.G., Mayor, S., and Klumperman, J. (2013). hVps41 and VAMP7 function in direct TGN to late endosome transport of lysosomal membrane proteins. Nat. Commun. *4*, 1361.

Pulecio, J., Petrovic, J., Prete, F., Chiaruttini, G., Lennon-Dumenil, A.M., Desdouets, C., Gasman, S., Burrone, O.R., and Benvenuti, F. (2010). Cdc42-mediated MTOC polarization in dendritic cells controls targeted delivery of cytokines at the immune synapse. J. Exp. Med. *207*, 2719–2732.

Puri, N., Kruhlak, M.J., Whiteheart, S.W., and Roche, P.A. (2003). Mast cell degranulation requires N-ethylmaleimide-sensitive factor-mediated SNARE disassembly. J. Immunol. *171*, 5345–5352.

Reefman, E., Kay, J.G., Wood, S.M., Offenhäuser, C., Brown, D.L., Roy, S., Stanley, A.C., Low, P.C., Manderson, A.P., and Stow, J.L. (2010). Cytokine secretion is distinct from secretion of cytotoxic granules in NK cells. J. Immunol. *184*, 4852–4862.

Stow, J.L., Manderson, A.P., and Murray, R.Z. (2006). SNAREing immunity: the role of SNAREs in the immune system. Nat. Rev. Immunol. *6*, 919–929.

Tiwari, N., Wang, C.C., Brochetta, C., Ke, G., Vita, F., Qi, Z., Rivera, J., Soranzo, M.R., Zabucchi, G., Hong, W., and Blank, U. (2008). VAMP-8 segregates mast cell-preformed mediator exocytosis from cytokine trafficking pathways. Blood *111*, 3665–3674.

Ward, D.M., Pevsner, J., Scullion, M.A., Vaughn, M., and Kaplan, J. (2000). Syntaxin 7 and VAMP-7 are soluble N-ethylmaleimide-sensitive factor attachment protein receptors required for late endosome-lysosome and homotypic lysosome fusion in alveolar macrophages. Mol. Biol. Cell *11*, 2327–2333.

Weinmann, A.S., Mitchell, D.M., Sanjabi, S., Bradley, M.N., Hoffmann, A., Liou, H.C., and Smale, S.T. (2001). Nucleosome remodeling at the IL-12 p40 promoter is a TLR-dependent, Rel-independent event. Nat. Immunol. *2*, 51–57.

Cell Reports, Volume *14*

Supplemental Information

The SNARE VAMP7 Regulates Exocytic Trafficking of Interleukin-12 in Dendritic Cells

Giulia Chiaruttini, Giulia M. Piperno, Mabel Jouve, Francesca De Nardi, Paola Larghi, Andrew A. Peden, Gabriele Baj, Sabina Müller, Salvatore Valitutti, Thierry Galli, and Federica Benvenuti

Supplemental experimental procedures

Mice

The animals used in this study were as follows: six to eight weeks old C57BL/6 mice were purchased from Harlan. OVA-specific, MHC class I and MHC class II restricted, TCR transgenic OT-I and OT-II mice were purchased from the Jackson Immuno Research Laboratories. Male VAMP7-deficient mice (Danglot et al., 2012) on a C57BL/6 background were compared with their male wild-type littermates. Mice were bred and maintained in sterile isolators. Animal care and treatment were conducted in conformity with institutional guidelines in compliance with national and international laws and policies (European Economic Community [EEC] Council Directive 86/609; OJL 358; December 12, 1987). Protocols were approved by the Italian Ministry of Health.

Cell culture

Dendritic cells were obtained from crude BM cells cultured in 24-well plates (2×10^6 cells/well) in complete IMDM (Gibco BRL) supplemented with 30% GM-CSF supernatants or 50 ng/ml Flt3L (R&D Systems). DCs were used for experiments between day 7 and 8, when expression of CD11c was higher than 80%. GM-derived cells were used for overexpression of fluorescently tagged proteins. For silencing, functional analysis and confocal microscopy conventional DCs from FLT3 derived cultures were isolated by negative selection using $B220^+$ microbeads (Miltenyi Biotec). For isolation of DCs from spleens, cell suspensions were obtained by digestion with Collagenase D (1.6 mg/ml; Roche) and DNase I (0.1 mg/ml; Roche) for 30 min at 37°C. Splenic DCs were enriched from total spleen cells by positive selection using $CD11c^+$ microbeads (Miltenyi Biotec). BM from I-A^b GFP mice (Boes et al., 2002), were a kind gift of Ana-Maria Lennon Dumenil, (Insitut Curie, Paris, France).

OT-I and OT-II cells were isolated from total lymph nodes suspension by negative or positive selection respectively using CD8 or CD4 purification kit (Miltenyi Biotec). Effector CD4+ T cells used to visualize IL12R clustering were generated by stimulating naïve CD4+T cells for 7 days with OVA class-II pulsed DCs (1:10 ratio) in the presence of recombinant IL-2. Human dendritic cells were generated as follows: PBMCs were isolated from the blood of healthy donors using the Ficoll gradient. From this population, monocytes were positively selected via CD14 beads from Miltenyi and then cultured in Mo-DC Differentiation Medium (Miltenyi) for seven days to generate immature Mo-DC.

TLR agonists

CpG-B (1826) oligonucleotide was bought from InVivoGen, San Diego, CA, LPS (*Escherichia coli* O55:B5) from Enzo Life Sciences, Inc. Human Mo-DC cells were stimulated with a cocktail of poli:IC (10ug/ml) and LPS (1ug/ml) for 5 hrs (In VivoGen).

Molecular cloning

SNAREs sequences cloned into an EGFP plasmid (Syntaxin6 and VAMP3 in -C2 vector with the GFP at the N-terminal, VAMP7 in -N1 vector with the GFP at the C-terminal) were a kind gift of JL Stow (University of Maryland, Brisbane). For the in vitro transcription compatibility, constructs were further subcloned into pcDNA3.1+ vectors bringing a T7 promoter at N-terminus of the protein sequences. Then plasmids were linearized cutting a site at the C-terminus in the non-coding region. P35-GFP and p35-SV5 were obtained by subcloning a recombinant p35 murine sequence (pORF5-mp35 purchased from Invivogen) in a pcDNA3.1+ together with a GFP and a SV5 sequence respectively at the C-terminal. A nucleotidic linker was kept between p35 and GFP sequences. RFP-VAMP7 vector was provided by T.Galli.

Silencing of VAMP7

Non-targeting siRNA and ON-TARGET plus siRNA targeting VAMP7 was purchased from Thermo Scientific (Dharmacon RNAi Technology), and used as control siRNA. ON-TARGET plus siRNA targeting VAMP7 were purchased by Thermo Scientific (Dharmacon RNAi Technology) and used as specific VAMP7 siRNA. BM-DCs were collected at day 5 and transfected with 2μM siRNA using the Amaxa Nucleofector according to the manufacturer's instructions. The transfected cDCs were collected and seeded into 24-well plates containing complete IMDM plus Flt3L. Cells were collected 48 h after transfection for sequent experiments.

RNA isolation, RT-PCR and qRT-PCR

Total RNA was isolated by TRI Reagent Isolation Kit (Sigma-Aldrich), following manufacturer's instructions. DNA was removed from isolated RNA fraction by a treatment with RNAse-free DNAse I (Fermentas Inc, Massachusetts, USA). Total RNA was retro-transcribed to cDNA by Moloney murine leukaemia RT (M-MLV-RT) in the presence of random hexamers (IDT). qRT-PCR was based on SYBR Green Master Mix (applied Biosystems) technology.

Primers used for qRT-PCR were as follows: *IL-12 p35* (for. 5'-GGCATCCAGCAGCTCCTCTC-3', rev. 5'-ACCCTGGCCAAACTGAGGT G-3'); *IL-12 p40* (for. 5'-TGGTTTGCCATCGTTTTGCTG-3', rev. 5'-ACAGGTGAGGTTCA CTGTTTCT-3'); *IL-6* (for. 5′-GAGGATACCACTCCCAACAGA-3′, rev. 5′-AAGTGCATCATC GTTGTTCAT -3′); *Stx6* (for. 5'-GGAGAGGTACAGAAAGCAGTCA-3', rev. 5'-CCCTGAAG GAGCTCTGTCCAT-3'); *VAMP3* (for. 5'-TGCTGCCAAGTTGAAGAGAAAG-3', rev. 5'-TGA TCCCTATCGCCCACATC-3'); *VAMP7* (for. 5'-ACCTTCGCCCCTCAGTCAAT-3', rev. 5'-G GCAAGGATAGTGGTTCCCC-3'); *GAPDH (*for. 5'-AGAAGGTGGTGAAGCAGGCATC-3', rev. 5'-AGAAGGTGGAAGAGTGGGAGTTG-3').

Western blot

Cells were washed and lysed with NP-40 plus protease inhibitors. The lysates were centrifuged at 13,000*g* for 10 min at 4 °C. The supernatants were boiled for 10 min and separated by SDS-PAGE using 12% polyacrylamide gel. Antibodies used: rabbit anti-VAMP3 and mouse anti-VAMP7 (provided by A. Peden, University of Sheffield, Sheffield, UK), mouse anti-Syntaxin 6 (BD Transduction Laboratories), mouse anti-V5 (Invitrogen), mouse anti-γ–tubulin (Sigma), rabbit anti-phospho $IKK_{\alpha,\beta}$, rabbit anti-IKKα, rabbit anti-phospho p38, rabbit anti-p38 (Cell Signalling), mouse anti-phospho $ERK_{1,2}$, mouse anti-ERK (Cell Signalling), anti-GAPDH-HRP (Sigma), goat anti-rabbit-HRP (Molecular Probes) and goat α-mouse-HRP (Pierce).

Cytokine secretion

IL-12 (p70) and IL-12 (p40) were measured with Ready-Set-Go! ELISA kit purchased from eBioscience; IL-6 and TNF-α were quantified with ELISA MAX kit from Biolegend; IFN-γ was measured with ELISA antibodies from BD Pharmigen.

FACS antibodies

The following antibodies for FACS analysis were purchased from BioLegend: FITC- and PE-conjugated anti-CD11c, PE-Cy5- and PE-Cy7-conjugated anti-I-A^b, PE-Cy5-conjugated anti-CD86, anti-CD40 and anti-rat isotype, FITC-conjugated anti-B220, anti-CD3 and anti-Gr-1, APC-conjugated anti-CD8α. Stained cells were acquired with a FACSAria III flow cytometer and analyzed with FLOWJO software (version 4.5.4; Tree Star Inc.).

Synapse formation, confocal analysis and in vivo imaging

VAMP7 (mouse) and VAMP3 (rabbit) antibodies were generated in house by A. Peden (Gordon et al., 2010). In some staining a mouse anti VAMP7 antibody purchased by

Creative Diagnostic (clone 25G579) was used. Rabbit anti-Rab27a was a kind gift of M. Seabra (Imperial College London, UK). In two cases, due to incompatibility of antibodies-host species (in the co-labeling with Rab6 and Rab11 in Fig.1C), VAMP3 was detected by overexpressing a GFP-tagged version of the SNARE. The following commercial antibodies were used: mouse anti-Syntaxin 6 (BD Transduction Laboratories), goat anti-EEA1 (BD Pharmigen), mouse anti-CD63 (MBL), rabbit anti-Rab11, rabbit anti-Rab6 (Santa Cruz), rat anti-IL-12 p40/p70 (BD Pharmigen), rabbit anti-Rab7 (Cell Signaling Technology), Texas-red phalloidin (Molecular Probes), rabbit anti-SNAP23 (Covalab), mouse anti-V5 (Invitrogen), rabbit anti-GFP (Molecular Probes). p35 tagged with SV5 or GFP was used depending on the species of the antibodies to be used in colabeling. Human p35 was detected using goat anti p70 antibodies (R&D). All secondary Alexa-tagged antibodies were obtained from Molecular Probes. ProLong® Gold Antifade Mountant with DAPI (Molecular Probes) was used as mounting medium. In some time lapse movies T cells were stained with 0.5 μM Bodipy 630 (Molecular Probes). Imaging was performed at room temperature when analyzing fixed cells or at 37°C when performing time-lapse microscopy. Confocal images and time lapses were acquired with a LSM510 META Axiovert 200M reverse microscope with an Objective Plan-Apochromat 63x/1.4 Oil DIC and an Objective Plan-Apochromat 100x/1.4 Oil DIC (Carl Zeiss, Inc.). A camera AxioCam HRc and LSM 510 acquisition software (Carl Zeiss) were used. Video 2 was acquired with an Axio Observer.Z1 microscope with an Objective Plan-Apochromat 63x/1.4 Oil DIC and a camera AxioCam 506, using the ZEN lite software (Zeiss). Image Z-stack projection of slides, three-dimensional reconstruction and image analysis were performed using Volocity® 3D Image Analysis Software (Perkin Elmer) and ImageJ (National Institutes of Health). For the colocalization mask in Fig 2B and E the pixels containing both staining above the threshold were used to generate a white channel. The threshold for the

different signals was automatically generated by the software, considering the PSF of wavelenghts and optics used. For the colocalization of the 3 channels in Fig 2C, the colocalization mask was first created for channel 1 and 2 and then superimposed to channel 3. The mask (white channel/only) created was super-imposed on the merged images to highlight the colocalization points using ImageJ (Fiji Version 1.49q). Manders of A (p40 or p35) on SNAREs or endosomal markers and persons' coefficient were calculated using Volocity software (Perkin Elmer).

Electron microscopy

Sections were examined using a Tecnai Spirit electron microscope (FEI Company) equipped with an Olympus-SIS Quemesa digital camera.

Statistical analysis

All statistical analyses were performed using GraphPad Prism®. The error bars show the SEM between mean values of independent experiments (as in the functional analyses and SNARE polarization analyses) or between values of single cells analyzed (SNARE/p35 co-localization at the IS and p35 distance from the PM). P-values were obtained by student's, Wilcoxon paired non parametric or Mann-Whitney *t* tests.

Supplementary Figure Legends

Figure S1. Kinetic of IL-12 induction in bone marrow derived DCs (BM-DCs), related to Figure 1.

(A) DCs were stimulated with CpG-B or LPS. Data show the relative expression of mRNA for IL-12/p70 (p35) or IL-12/p40 (p40) at different times post-stimulation. Bars show mean±SEM of three independent experiments. ***:p<0,0001, Student's *t* test. *(B*) Kinetic of IL-12/p40 and p70 protein secretion upon CpG-B stimulation. Cell culture supernatants were harvested at the indicated time points and quantified by ELISA. Bars show the mean±SEM of two independent experiments.

Figure S2. Validation of p35-tagged constructs, related to Figure 2.

(A) p35-SV5 and mock-transfected DCs were stimulated or not with CpG-B for 7 hours. Cell lysates were immunoblotted with anti-SV5. g-tubulin was used as loading control. *(B)* DC overexpressing p35-SV5 were stimulated or not with CpG-B for 24 hours. Cell culture supernatants were immunoblotted with anti-SV5. *(C)* p35-SV5-transfected DCs were stimulated for 3 hours with CpG-B. Representative plane showing co-localization of SV5 (green) with the endogenous IL-12/p40 subunit (red). *(D,E)* p35-SV5- *(D)* and p35-GFP- *(E)* transfected DCs were stimulated with CpG-B for 8 hours. Cell culture supernatants were immunoprecipitated with anti-SV5 and immunoblotted with anti-p40. Mock-transfected DCs were used as negative control. *(F)* DCs were co-transfected with p35-SV5 and p35-GFP. Representative plane showing intracellular co-localization of the two proteins. (g). *(G)* Cells transfected with p35-SV5 were counter-labeled with antibodies against p40 and VAMP7. Single confocal planes showing single channels, color merges of channels 2 by 2 and a colocalization mask showing colocalization for the 3 channels are shown.

Figure S3. Phenotype of VAMP7 KO DCs, related to Figure 3.

A) BM-DCs lysates from WT and VAMP7KO mice were analyzed by immunoblotting for VAMP7 expression; γ-tubulin was used as loading control. (*B*) Representative dot plots of conventional DCs in the spleen. $B220^-/CD3^-/Gr\text{-}1^-$ splenocytes were labelled with antibodies against $CD11c^+$ and $I\text{-}A^b$ (left) or CD8a (right) *(C)* Frequency of total conventional DCs ($CD11c^+/I\text{-}Ab^{high}$, left panel) and CD8α positive and negative DCs (right panel) in the spleen of WT and VAMP7KO mice. Each data point represents one mouse. n.s., not significant, Student's t test.

Figure S4. TLR9 signaling and DCs maturation are not affected by VAMP7 deficiency, related to Figure 3.

(A) Immunoblot analysis of WT and VAMP7KO BM-DCs stimulated for 10, 30 or 60 min with CpG-B and probed with Abs against p-IKK, p-ERK and p-p38. GAPDH, total ERK and total p38 were used as loading controls. One representative experiment out of three with similar results is shown. *(B)* Expression of maturation markers in bone marrow (BM) and splenic DCs post CpG-B stimulation. WT, green histograms; VAMP7KO, blue histograms; dashed lines, isotype control. *(C)* Mean fluorescence intensities (MFI) for the indicated maturation marker. Data represent mean±SEM of four independent experiments. p values were determined by Student's t test. n.s., not significant. *(D)* mRNA expression of p35, p40 and IL-6 was measured by qPCR in BM-DCs. Data are mean±SEM of two independent experiments.

Figure S5. Selection of siRNA oligos for VAMP7 knockdown, related to Figure 3.

(A) Cells were transfected with a siRNA targeted against VAMP7 (siVAMP7) or with an unrelated siRNA (CTRL). The level of protein expression was assessed by Western Blot 48 hrs post transfection. On the right, densitometry quantification of VAMP7 expression, one representative of 4 blots with similar results. *(B)* Control siRNA does not affect protein secretion. DCs transfected with mock or with not targeting siRNAs (#1-6) were stimulated for 6 hours with CpG-B and the levels of secreted IL-12/p70 were measured. SiRNA#1 was chosen for the experiments. *(C)* DCs transfected with non-targeting siRNA#1 (siIrrelevant) and a VAMP7-targeting (siVAMP7) siRNA were labelled after 48 hours and stained with with Annexin V and 7-AAD to assess viability. *(D)* Control (black line) and VAMP7-silenced (green line) DCs were stimulated or not (n.s.) with CpG-B for 15 hours and expression of maturation markers CD86, I-A^b and CD40 evaluated by FACS. One representative of three experiments is shown. *(E)* Cytokines gene induction in control and VAMP7 knock-down cells was determined by RT-PCR at 3 hours post stimulation. Mean values±SEM of four independent experiments, n.s. not significant, Student's *t* test.

Figure S6. Synaptic clustering of p35 in human DCs, related to Figure 4.

(A) Representative confocal planes showing the distribution of endogenous p35 in human Mo-DCs in synapse with $CD4^+$ T cells. Mo-DCs were loaded with 1 mg/ml of superantigens (SEB and TSST1) and mixed with CD3/CD28 activated $CD4^+$ T cells. After 30 min of

interaction, cells were fixed, labeled with antibodies against human p35, VAMP7 or Rab27 and analyzed by confocal microscopy. Insets show a 3x magnification of the synaptic regions. All bars shown in micrographs correspond to 5mM.

Legends to supplemental Movies

Movie S1. Related to Figure 5A.

Time-lapse confocal microscopy of VAMP7-RFP expressing DC during formation of conjugates with naïve T cells stained with membrane dye Bodiby630 (blu). The movie shows that cluster of VAMP7 polarize toward the interaction plane upon a T cell contact. Interestingly, VAMP7 transiently moved away from the first T cell to travel towards a second T cell contacting the same DCs, and repolarized again to the first contacted T cell within few min. Frames were acquired every 30s for 50 min.

Movie S2. Related to Figure 5D.

Epifluorescence imaging of DC transfected with p35-GFP in synapse with a $CD4^+$ T cell. The position of the T cell is indicated by white dotted lines. Imaging was started short after contact formation. The time-lapse series show bright fast moving dots of p35 in the cell periphery and a highly motile enrichment of vesicles underneath the synaptic membrane. Frames were taken every 400 ms for 2 min 45 sec.

Movie S3. Related to Figure 5D.

High magnification of Movie S2 in the synaptic region shows $p35^+$tubules docking at the plasmamembrane.

Movie S4. Related to Figure 5E.

Time-lapse confocal microscopy of DCs co-transfected with p35-GFP and VAMP7-RFP, forming a conjugate with a T cell (blu). Frames were taken every 30s for 30 min. Video to Fig.5.

A

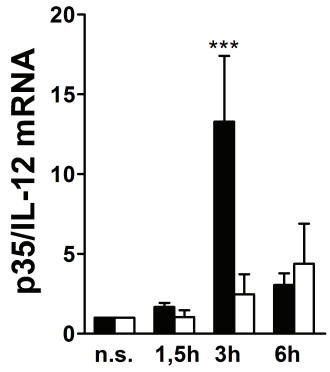
p35/IL-12 mRNA
20
15
10
5
0
***
n.s.
1,5h
3h
6h

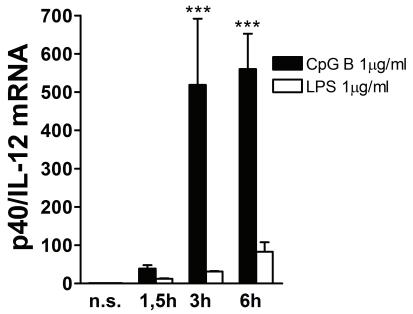
p40/IL-12 mRNA
700
600
500
400
300
200
100
0
***
***
n.s.
1,5h
3h
6h
CpG B 1μg/ml
LPS 1μg/ml

B

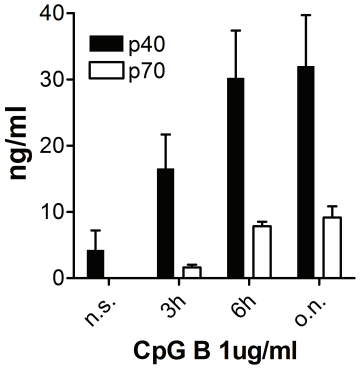
ng/ml
40
30
20
10
0
p40
p70
n.s.
3h
6h
o.n.
CpG B 1ug/ml

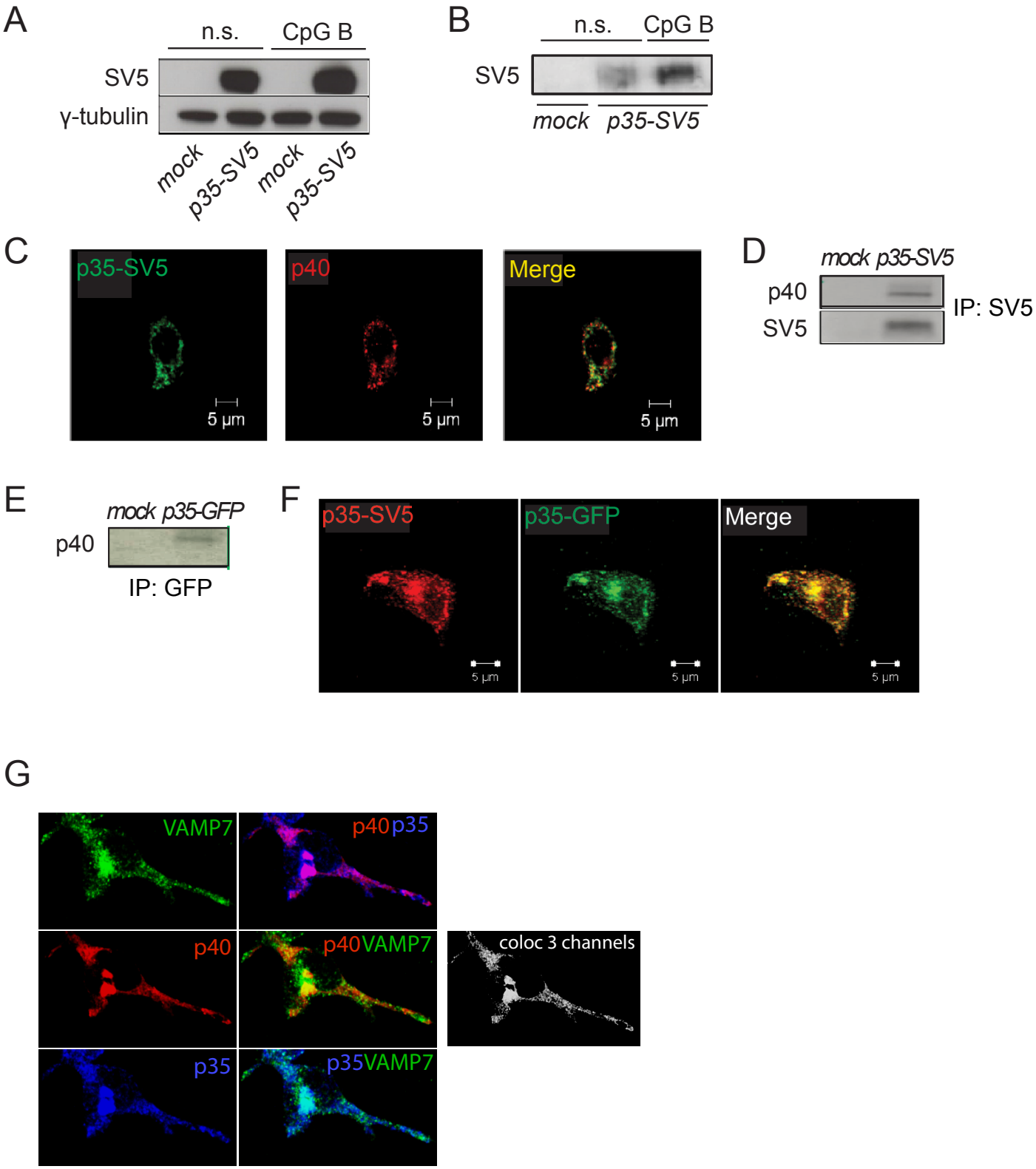
A
n.s.
CpG B
SV5
γ-tubulin
mock
p35-SV5
mock
p35-SV5
B
n.s.
CpG B
SV5
mock
p35-SV5
C
p35-SV5
p40
Merge
5 µm
5 µm
5 µm
D
mock p35-SV5
p40
SV5
IP: SV5
E
mock p35-GFP
p40
IP: GFP
F
p35-SV5
p35-GFP
Merge
5 µm
5 µm
5 µm
G
VAMP7
p40 p35
p40
p40 VAMP7
coloc 3 channels
p35
p35 VAMP7

Figure S2

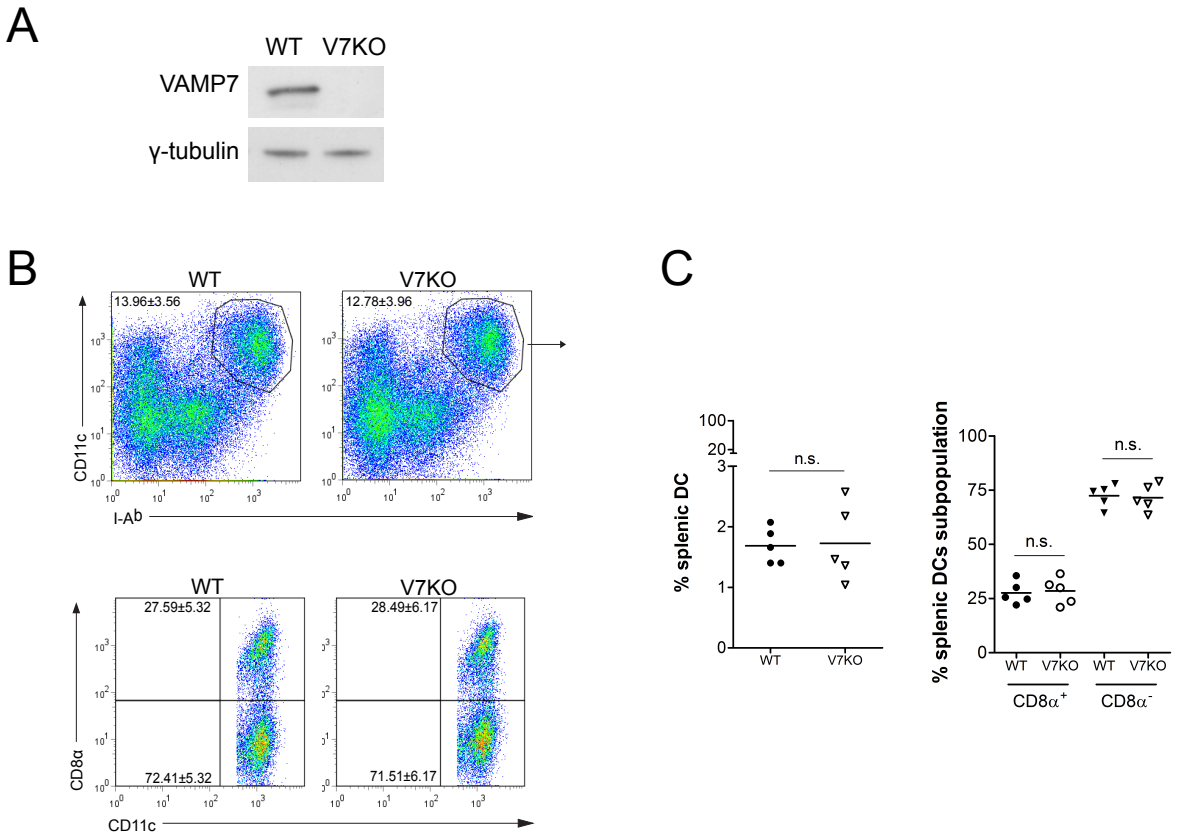
A
WT
V7KO
VAMP7
γ-tubulin
B
WT
V7KO
13.96±3.56
12.78±3.96
CD11c
I-Ab
WT
V7KO
27.59±5.32
28.49±6.17
72.41±5.32
71.51±6.17
CD8α
CD11c
C
% splenic DC
n.s.
WT
V7KO
% splenic DCs subpopulation
n.s.
n.s.
WT
V7KO
WT
V7KO
CD8α+
CD8α-

Figure S3

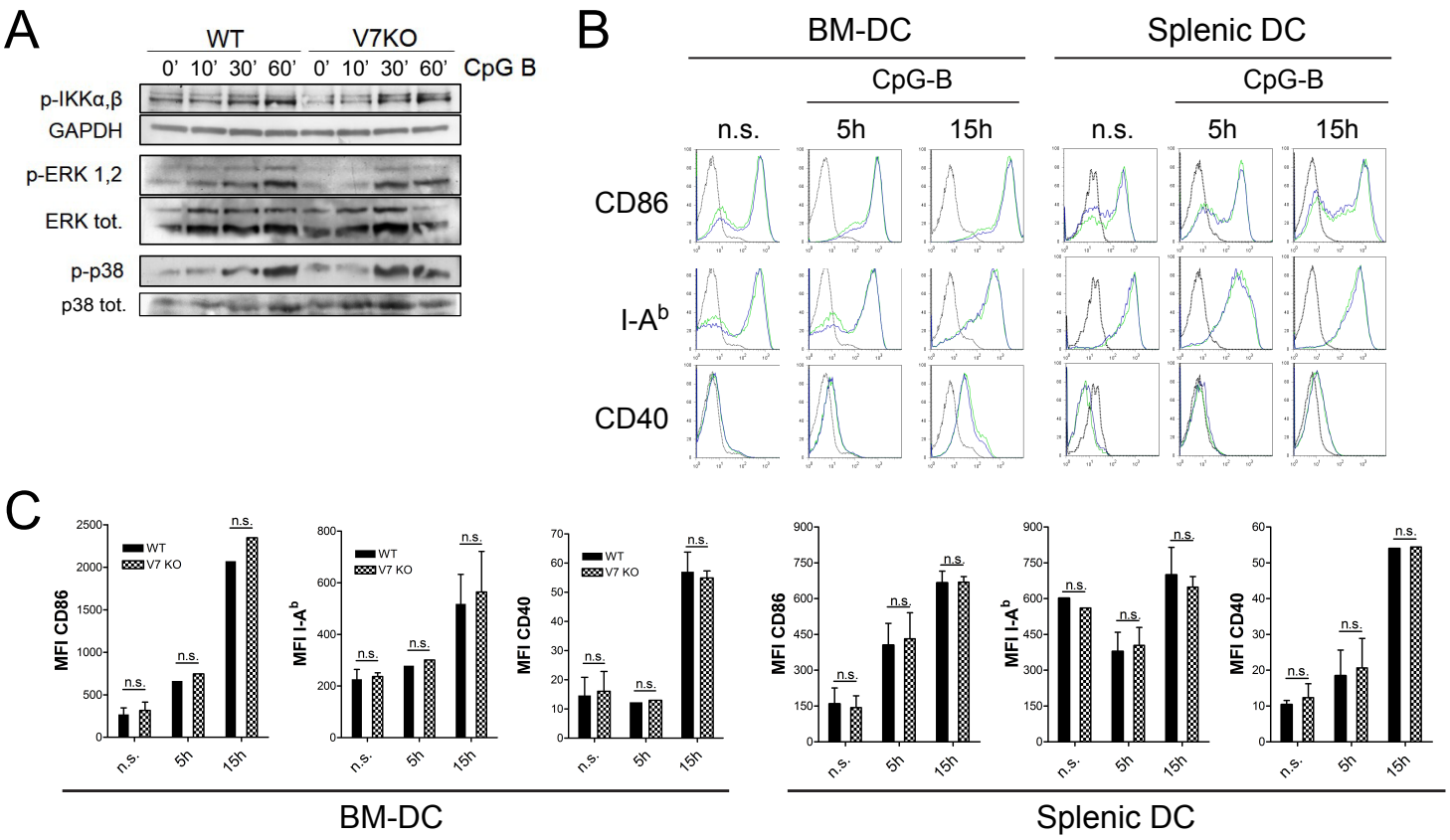
A
WT
V7KO
0' 10' 30' 60' 0' 10' 30' 60' CpG B
p-IKKα,β
GAPDH
p-ERK 1,2
ERK tot.
p-p38
p38 tot.
B
BM-DC
Splenic DC
CpG-B
n.s.
5h
15h
CD86
I-Ab
CD40
C
MFI CD86
MFI I-Ab
MFI CD40
WT
V7 KO
n.s.
5h
15h
BM-DC
Splenic DC

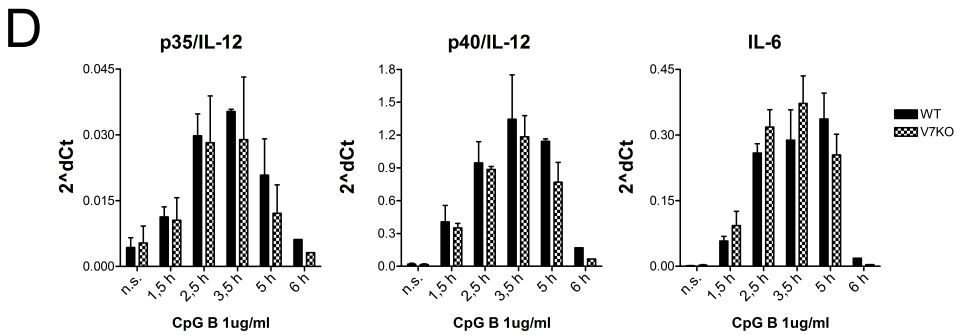
D
p35/IL-12
p40/IL-12
IL-6
2^dCt
WT
V7KO
n.s.
1,5 h
2,5 h
3,5 h
5 h
6 h
CpG B 1ug/ml

Figure S4

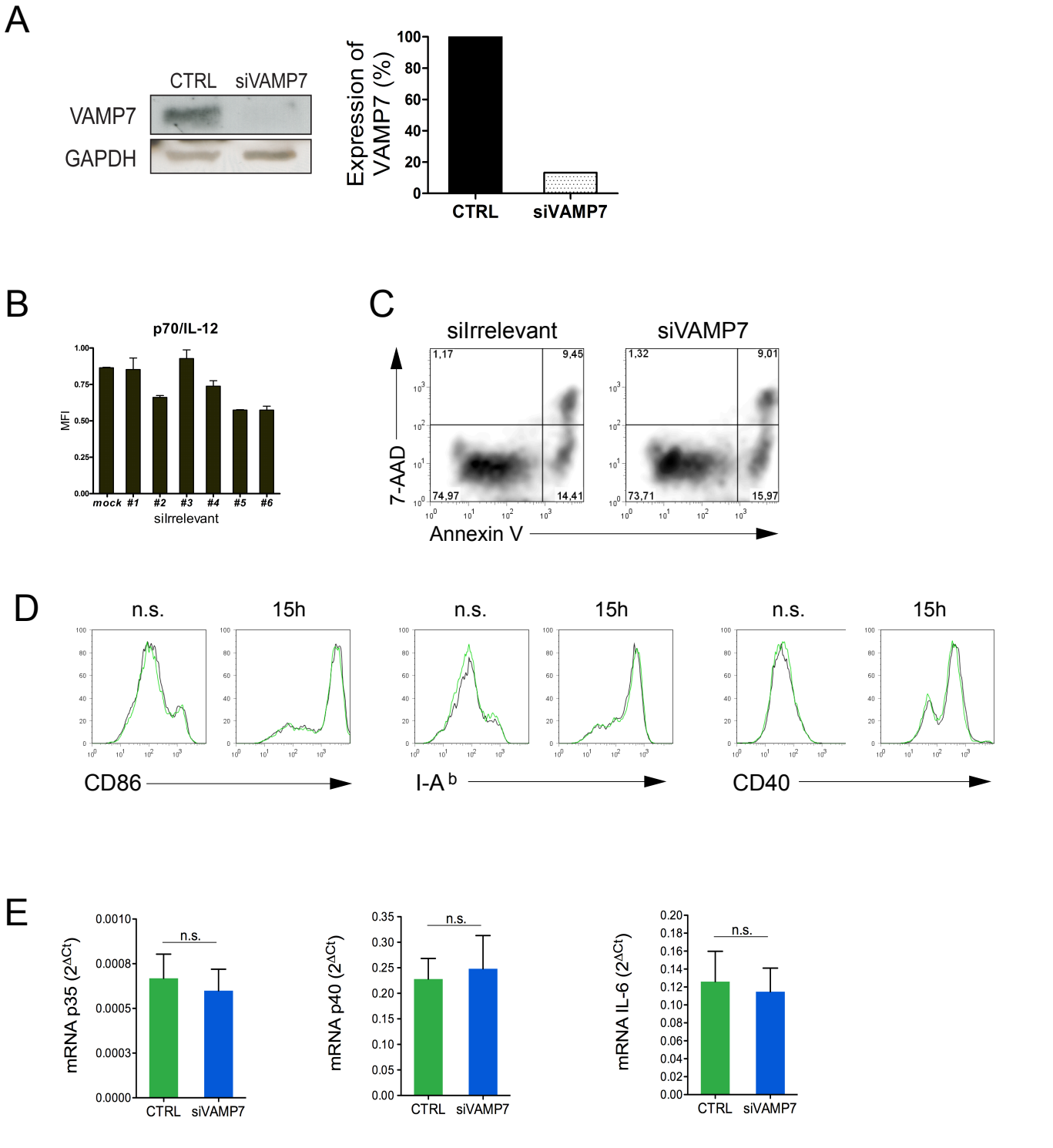
A
CTRL
siVAMP7
VAMP7
GAPDH
Expression of VAMP7 (%)
100
80
60
40
20
0
CTRL
siVAMP7
B
p70/IL-12
MFI
1.00
0.75
0.50
0.25
0.00
mock
#1
#2
#3
#4
#5
#6
silrrelevant
C
silrrelevant
siVAMP7
1,17
9,45
74,97
14,41
1,32
9,01
73,71
15,97
7-AAD
Annexin V
D
n.s.
15h
CD86
I-A b
CD40
E
mRNA p35 (2ΔCt)
0.0010
0.0008
0.0005
0.0003
0.0000
n.s.
CTRL
siVAMP7
mRNA p40 (2ΔCt)
0.35
0.30
0.25
0.20
0.15
0.10
0.05
0.00
mRNA IL-6 (2ΔCt)
0.20
0.18
0.16
0.14
0.12
0.10
0.08
0.06
0.04
0.02
0.00

Figure S5

A

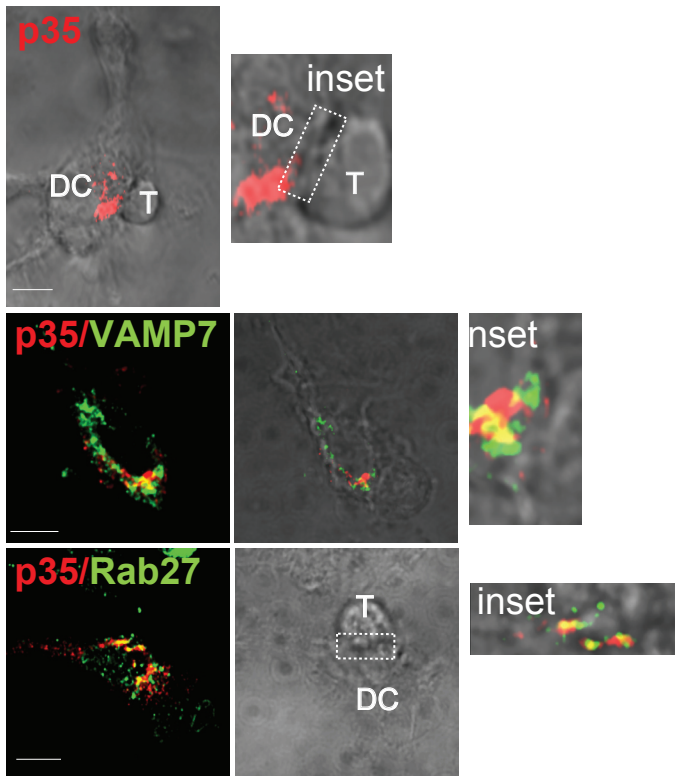

Figure S6